63-3-6

hp associates • 2900 park boulevard • palo alto, california • DA 1-8510

AFCRL-63-113

INVESTIGATION OF HOT ELECTRON EMITTER

-hp associates-
2900 Park Boulevard
Palo Alto, California

Contract No. AF19(628)-1637
Project No. 4608
Task 460804

SCIENTIFIC REPORT NO. 3

December 1, 1962 - February 28, 1963

Prepared
for

AIR FORCE CAMBRIDGE RESEARCH LABORATORIES
OFFICE OF AEROSPACE RESEARCH
UNITED STATES AIR FORCE
BEDFORD, MASSACHUSETTS

Requests for additional copies by Agencies of the Department of Defense, their contractors, and other Government Agencies should be directed to the:

ARMED SERVICES TECHNICAL INFORMATION AGENCY
ARLINGTON HALL STATION
ARLINGTON 12, VIRGINIA

Department of Defense contractors must be established for ASTIA services or have their "need to know" certified by the cognizant military agency of their project or contract.

All other persons and organizations should apply to the:

U. S. DEPARTMENT OF COMMERCE
OFFICE OF TECHNICAL SERVICES
WASHINGTON 25, D. C.

TABLE OF CONTENTS

ABSTRACT

The electrical properties of gold-silicon barriers have been studied experimentally in some detail. The reverse leakage current of these barriers is shown to be caused by lowering of the barrier due to the image force effect. The thermal activation energy of the saturation current was found to be 0.799 eV, identical to the height of the Au-Si barrier. The barrier height, saturation current density, and ideality of Pt, Pd, Ag, Ni and Cu barriers to Si are also presented.

Two methods for fabricating hot electron triodes are described. Large area structures, made by pressing together a silicon-gold-silicon sandwich, do not exhibit triode characteristics and are limited by particulate matter and deviations from flatness. Triodes with point contact emitters of silicon and gallium arsenide have been fabricated and their current-voltage characteristics are presented. Current transfer ratios as high as 0.75 have been observed.

I. ELECTRICAL CHARACTERISTICS OF GOLD-SILICON BARRIERS

A theoretical treatment of the electrical characteristics of metal-semiconductor rectifying barriers was presented in Scientific Report No. 1. Some preliminary experimental results on the temperature dependence of the current-voltage and capacity-voltage characteristics of Au-Si barriers were also given. These experiments have been refined, and are described here in detail. In addition, the reverse leakage characteristics of these barriers have been carefully examined and are now rather well understood. Gold-silicon barriers have been more thoroughly examined than other metal-silicon barriers because of the ease of using gold and because of its relatively long hot electron range. However, it is now clear that gold barriers are more complex in some respects than those of some of the other metals which are described in Section II. It is not known, at this time, how this greater complexity will affect the characteristics of hot electron triodes.

A. I-V Characteristics and Image Force Barrier Lowering

The I-V characteristics of an evaporated Au-Si barrier (4×10^{15} donors/cm^3) are shown in Figure 1. This barrier was made by the techniques described in Scientific Report No. 1 and is typical of the better barriers on the Si slice. The curve can be approximated for forward bias greater than 0.1V by the familiar diode equation

$$I = I_s [\exp(qV/nkT)-1] \quad (1)$$

where $I_s = 1.42 \times 10^{-10}$A. Note, however, that n = 1.15 at low currents and n = 1.04 at high currents. Furthermore, for $|V| < -0.1$v, the data cannot be fit by this equation for any fixed value of n. The reverse current does not saturate properly even at 0.5v. These features are present to this extent in all Au-Si barriers studied.

The reverse characteristic of this barrier is shown in Figure 2 for reverse voltage from 0.1v to 90v. The I-V dependence at high reverse voltages is believed to be caused by lowering of the barrier due to the force between an electron in the semiconductor and its image in the metal, as indicated in Figure 3. The reverse current can then be written as

$$I_R = I_{SR} \exp(q\delta/kT) \quad (2)$$

where

$$\delta = (qE_s/\kappa_h)^{1/2} \quad (3)$$

and

$$E_s = [8\pi N_d q(V_b-V)/\kappa_s]^{1/2} \quad (4)$$

These equations use electrostatic units and E_s is the field at the surface, N_d is the donor density, V_b is the built-in voltage, and κ_s and κ_h are the static and high frequency dielectric constants, respectively. The κ_h must be used in

Equation (3) because the electrons move through the first few angstroms so rapidly that dipole and ionic polarization of the lattice does not occur. However, for silicon $\kappa_s=\kappa_h=12$, since the polarizability is purely electronic. Electronic polarizability is usually considered to become ineffective for times less than about 10^{-15} seconds, but this is just the time required for an electron moving at 10^8cm/sec to go 10Å so that it is not evident in this case whether a value of 12 or 1 should be used for κ_h. The current has been calculated for both values using Equation (2) and is shown in Figure 2, in which I_{SR} has been chosen to obtain a fit at 20v. It is apparent from Figure 2 that 12 is the correct value for κ_h in this case. Furthermore, the excellent agreement for $10<V<90$v demonstrates that image force barrier lowering is the major fundamental mechanism of reverse current in these barriers.

The value of I_{SR} used to obtain the fit above for $\kappa_h = 12$ was 4.56×10^{-10}A. The barrier lowering at V = 0 is $\delta = 17.2$ mv, and δ approaches zero at high forward voltage. This increasing barrier height with forward voltage explains the value of $n = 1.04$ at large forward voltages but cannot explain the higher value of n at low voltages or gross deviation from the ideal diode equation for $|V|<0.1$v. Thus, the I-V characteristics of Au-Si barriers may be considered in three regions: the region of high forward voltage where the equation

$$I = I_{SF}[\exp(qV/nkT)-1]$$

is a good description; the region of high reverse voltage where Equation (2) is a good description and $I_{SR} > I_{SF}$; and the region of $-5v < V < 0.3v$ where the behavior is more complex and is not yet understood.

B. Temperature Dependence of the Electrical Characteristics

The internal barrier height of Au-Si barriers was found to be 0.80 eV both by the photoelectric measurement and by the capacity-voltage intercept measurement (Scientific Report No. 1). It is useful to determine whether the I_S has a thermal activation energy equal to this barrier height, particularly since the I-V characteristic is anomalous near the origin. Some preliminary data in Scientific Report No. 1 indicated an activation energy, E_{th}, of 0.687 eV, which was interpreted as being due to an "excess current" in the anomalous region of the I-V characteristic which was thought to be space charge recombination current. However, the three points in the I_S vs. 1/T curve did not lie on a straight line, and the activation energy corresponding to the two higher temperatures was 0.85 eV. The I_S at the lowest temperature most likely does include some excess current, but it is the behavior of the current at the higher temperatures which is of basic interest. The temperature dependence experiments have been repeated at room temperature and above on a very pure crystal, leading to $E_{th} = 0.799$ eV and to the conclusion that the anomalous region of the I-V characteristic is not due to space charge recombination.

The experiment was done on nominally dislocation-free n-type silicon with $N_d = 4 \times 10^{15}/cm^3$. The wafer was mounted on a fixture which made contact to one of the diodes. The fixture was kept in a special oven in an argon atmosphere during the entire experiment. The C-V and I-V characteristics were measured at 22, 43.7, 70.5, and 100.6°C, and re-checked at 22°C to insure that the characteristics were reproducible.

The plot of $1/C^2$ vs. V is shown in Figure 4 for each temperature. The lines indicate a shift with temperature due to the variation of V_F, the difference between the Fermi level and the bottom of the conduction band, and there is a slight change in slope at the two highest temperatures. This may be due to donors which have a larger ionization energy than normal, and would then represent a 35% larger value of N_d at 100.6°C than at 22°C. As described in Scientific Report No. 1, the value of internal barrier height, V_i, may be calculated from

$$V_i = V_o + kT/q + V_g/2 - (kT/q) \ln N_d/n_i$$

where V_o is the intercept from Figure 4 and V_g is the band gap voltage.

TABLE I

DETERMINATION OF THE INTERNAL BARRIER HEIGHT

T	n_i	V_g	V_o	V_i
22°C	$9 \times 10^9/cm^3$	1.090v	0.560v	0.795v
43.7°C	5.10×10^{10}	1.080	0.525	0.784
70.5°C	3.16×10^{11}	1.069	0.515	0.799
100.6°C	1.92×10^{12}	1.057	0.485	0.800

The calculated value of V_i for each temperature is shown in Table I and has an average value of 0.795v. The determination of V_o from Figure 4 can be made to within 0.01v and this uncertainty is the main cause of scatter in the values of V_i given in Table I. This does confirm the value of V_i given earlier, and establishes that V_i is independent of temperature.

The I-V characteristics are shown in Figures 5 to 8 for the four temperatures. The non-ideal characteristics exist at all temperatures, although the value of n at low voltage does decrease from 1.20 at 22°C to 1.09 at 100.6°C. In each case, $n = 1.04$ for $V > 0.3v$, except at 100.6°C where series resistance interferes at 0.3v. The saturation current obtained by extrapolation of the forward curve is plotted vs. 1/T in Figure 9 for each temperature. These points can be fitted rather well with a straight line which yields an activation energy $E_{th} = 0.799$ eV. This value of E_{th} is essentially identical to the internal barrier height described above, which indicates that the current is due to electrons which go over the top of the barrier. This argues against the interpretation of the anomalous region of the I-V curve as being dominated by an "excess current" component since the "excess current" and the "normal" hot electron current have the same temperature dependence. It seems preferable then to regard this anomalous region as an inherent feature of hot electron flow in Au-Si barriers. This point of view is supported by the observation, described in detail in the next section, that Pt-Si barriers

exhibit ideal I-V characteristics even though they have saturation current densities as low as those of Au-Si barriers.

The exact temperature dependence that one would expect for Au-Si depends on which mechanism determines the I-V characteristics. For a barrier with ideal I-V characteristics, the current density can be described as in Scientific Report No. 1, by the relation

$$j = qv_o N_c \exp(-qV_i/kT)[\exp(qV/kT)-1] \qquad (6)$$

where v_o is the average thermal electron velocity in the semiconductor (probably of the order of $[kT/2\pi m_e]^{1/2}$) and N_c is the effective density of states in the conduction band

$$N_c = (2/h^3)(2\pi m_e^* kT)^{3/2}$$

If Equation (6) is correct in detail, then $j_s \alpha T^2 \exp(-qV_i/kT)$; and if $\ln(I_s/T^2)$ is plotted vs. $1/T$, one should obtain an activation energy equal to V_i. This was done for the above data and an activation energy of 0.75 eV was obtained, which is about 30 mv less than the internal barrier height V_i (including barrier lowering due to image forces). It is felt that this discrepancy does not require a change in the interpretations given above, since the I-V characteristics show that the model leading to Equation (6) is over-simplified for Au-Si barriers.

II. CHARACTERISTICS OF BARRIERS OF VARIOUS METALS TO SILICON

The properties of several metal-to-silicon barriers have been examined. The information obtained from this effort has aided our understanding of metal-silicon barriers in general. In addition, hot electron triodes should be made using other metals, as well as gold, and the barrier height and the degree of ideality of each metal-Si barrier should be known.

The I-V and C-V characteristics of a Pt-Si barrier are shown in Figures 10 and 11, respectively. The Pt barrier has essentially ideal I-V characteristics with n = 1.02. This slight deviation from n = 1.0 can be explained by the small change in barrier height with bias due to the image force effect, as discussed in Section I. The curvature in the I-V characteristic above 10^{-4}A for this and all the other barriers shown is caused by series resistance. The ideality of the I-V curve is indicated not only by the value of n, but also by the saturation of the reverse current in the region V<0.5v and the agreement of that saturation value with the one obtained by extrapolating the forward current.

Both Pt and Au barriers were made on this slice of Si to determine whether the non-ideality could be caused by space charge recombination currents. The Au barriers were identical to those described in Section I. If the "excess current" in Au barriers were due to space charge recombination, then that current would also dominate in Pt barriers. Since the saturation current of Pt is smaller than that of Au and the curve is

ideal, the "excess current" of Au barriers cannot be due to space charge recombination.

The I-V and C-V characteristics of Pd, Ag, and Cu barriers are shown in Figures 12 through 17. The I-V characteristic of a Ni barrier is shown in Figure 18. The C-V curve for this Ni barrier was not useful because the N_d was varying slightly with depth so that the V_o could not be obtained accurately. The I-V characteristic is still meaningful for this Ni barrier because the current is independent of doping, whereas the determination of V_o requires extremely uniform doping.

TABLE II

PROPERTIES OF SOME METAL-SILICON BARRIERS

	n	j_s (A/cm^2)	V_i
Au	1.15	7.5×10^{-7}	0.80
Pt	1.02	5.9×10^{-7}	0.77
Pd	1.08	9.5×10^{-6}	0.72
Ag	1.08	2.3×10^{-5}	0.67
Ni	1.03	1.2×10^{-3}	--
Cu	1.05	1.4×10^{-3}	0.58

The salient features of these barriers are summarized in Table II, along with the corresponding information for Au barriers from Section I. Note that the value of n is a good quantitative indication of the non-ideality in each case, and

that Pt and Ni are very ideal; Cu, Pd and Ag less so; and Au quite non-ideal. The values of j_s for Au, Pt, and Pd have been independently reproduced several times and are reliable within a factor of about 2; whereas, the j_s of Ag, Ni and Cu are less well established. The V_i of Ag, Ni, and Cu are similarly subject to some uncertainty. The saturation current density is plotted in Figure 19 as a function of the internal barrier height, V_i. Since j_s is proportional to $\exp(-qV_i/kT)$, the points should fit a line of slope q/kT. As indicated, the fit is satisfactory.

III. HOT ELECTRON TRIODES

A comparison was presented in Scientific Report No. 2 of several types of hot electron triodes, differing only in the type of emitter utilized. It was concluded that the semiconductor metal-semiconductor (SMS) triode with a Schottky barrier emitter offered the highest emitter figure-of-merit (g_e/C_e) and the highest maximum oscillation frequency at a given current density. Accordingly, a significant portion of our experimental effort has been directed toward the fabrication and analysis of SMS hot electron triodes. In addition to the potential practical importance of such a triode, the analysis of triode characteristics provides one of the best ways of understanding the hot electron emitting properties of a Schottky barrier, just as the invention and study of transistor action greatly aided the understanding of pn junctions.

Finally, the SMS triode offers one of the best ways of exploring a relatively new area of solid state physics, viz., the behavior of hot electrons in metals.

Three methods for the fabrication of SMS triodes have been employed thus far. The first method consists of pressing a very flat semiconductor (emitter) against a metal-coated, flat semiconductor (collector). This method has the important advantage of utilizing single-crystal semiconductors of known area which make barriers which are now rather well understood. The second type of SMS triode consists of a point emitter which lightly contacts a metal layer which is evaporated on the collector. This structure has some serious limitations, but it is the easiest to fabricate and has yielded some valuable information. The third type of SMS triode consists of a polycrystalline semiconductor deposited on a metal base which is evaporated on a single crystal semiconductor substrate. The work on this last type is now being emphasized and will be described in detail in Scientific Report No. 4.

A. Flat Emitter Triode Structures

The fabrication of a large area triode with single crystal emitter and collector requires that the crystal surfaces be extremely flat and clean in order that they touch everywhere when pressed together. Silicon wafers have been polished flat to within 1000-2000Å across a one-inch diameter. This amounts to a deviation from flatness of 5-10Å across the

5 mil diameter emitters used in device fabrication. The processing steps of thinning the thick, polished wafers, contact preparation, and oxidation have been investigated to determine their influence on wafer flatness. It was found that the best results were obtained when the wafer was oxidized to remove the polishing damage and the back was prepared by etching, diffusing phosphorous into it and contacting with evaporated gold. Lapping or alloying on the back resulted in excessive warpage.

Using these techniques, several Si-Au-Si structures were assembled. In most cases, a point contact was obtained, as inferred by the emitter capacity and series resistance, in spite of the precautions to avoid dust or other particulate matter. These unintentional point contact emitter structures usually showed triode action, but the collector characteristics were quite unstable. In those few structures in which a majority of the emitter surface was making intimate contact with the metal base, the emitter I-V and C-V characteristics were highly abnormal and no triode action was observed.

Another method for fabrication, which was briefly investigated, was the pressing together of two large, thin, gold-coated silicon flats and allowing the gold to bond to itself. The devices would then be etched apart. Particulate matter was found to limit bonding although occasionally a bonded piece was obtained. No triode action was observed on any device which was believed to have a large area contact emitter.

B. Point Contact Emitter Structures

Since the flat emitter structures which exhibited triode action were those which made only a point contact to the metal and their characteristics were erratic, we decided to make a triode structure with a mechanically stable point contact emitter. The emitters were made by etching three points on the front of the 0.020" square chips, one near each of three corners. This tripod structure was chosen to give the greatest mechanical stability of the emitter point. One of the three points contacts the metal base, and the other two are on an oxide layer, as depicted in Figure 20. The point contact emitter shares with the flat emitter structure the advantage of using single crystal semiconductors, but the contact area of the point emitter is very small and unknown.

B.1. Silicon Point Emitters

The collector characteristics of a silicon point emitter triode which has a relatively high gain is shown in Figure 21. This triode has a collector of 0.86 ohm-cm n-type Si, a 200Å thick Au base layer, and an emitter of 0.19 ohm-cm n-type Si. The collector characteristics, shown in Figure 21, are very similar to those of an npn transistor, except for the higher collector leakage and the higher emitter series resistance which causes the large voltage offset of each successive trace in the grounded emitter family. The value of α is about 0.5 and it is decreasing slightly with increasing current.

Most Si-Au-Si point emitter triodes do not exhibit a value of α as high as 0.5. This is not due to low transport efficiency, since the α does not vary in a regular manner with base width. Furthermore, the α varies with point pressure, the highest values of α being obtained with very light pressure. The α is also sensitive to mechanical shock and for a given structure can be changed from about 0.5 to about 10^{-3}. These shocks are postulated to cause a change in the location or area of that part of the emitter which is contacting the base layer. One possible reason for this large α variation is that edge current, which is not hot electron current and is proportional to the contact perimeter, dominates the hot electron current, which is proportional to the contact area. However, the observation that the emitter current is insensitive to change in ambient gases (HF, NH_3, and H_2O) tends to argue against this explanation.

Another reason for this α variation is that the emitter electron affinity varies over its surface so that the emitter barrier height is sometimes less than the collector barrier height. The emitter barrier height cannot be measured directly in the usual way because the contact area capacity is less than that of the stray capacity of the nearly contacting region, and because the contact area is unknown.

It was also observed that relatively high gain units could be made using germanium collector material which has a lower barrier height to gold than does silicon. The problems

of surface instability associated with germanium, however, make it a difficult material to use as an analytical tool. To insure that barrier height differences are not a gain limiting mechanism, the emitter semiconductor should have an electron affinity smaller than that of the collector.

B.2. Gallium Arsenide Point Emitters

Gallium arsenide has been investigated for use as an emitter. Diodes were fabricated by evaporating 5.1 mil diameter gold dots onto the freshly etched ($\bar{1}\bar{1}\bar{1}$) arsenic side of gallium arsenide. The internal barrier height is obtained from the capacitance-voltage characteristics (Figure 22) as:

$$V_i = V_o + \frac{kT}{q} + V_F$$

where, V_o is the intercept of the $1/C^2$ vs. V plot, and V_F is the energy position of the Fermi level below the conduction band edge. From Figure 23, the intercept $V_o = 0.89$ volts corresponds to a barrier height $V_b = V_o + kT/q = 0.916$. The value of V_F may be obtained from:

$$\frac{N_D}{N_C} = e^{-V_F/kT}$$

where, the number of donors $N_D = 4.6 \times 10^{16} cm^{-3}$ and N_C, the effective density of states in the condution band, is taken to be $4.7 \times 10^{17} cm^{-3}$. This yields an internal barrier height of $V_i = 0.977$ volts. This barrier is 0.177 volts higher than that of Au-Si, thus GaAs should be a suitable emitter for a triode with a Si collector.

The current-voltage characteristics of this same diode are shown in Figure 23. This curve may be described for forward bias greater than about 150 mv by the equation $I = I_s[\exp(qV/nkT)-1]$, where $n = 1.1$ and $I_s = 1.5 \times 10^{-12}$A. The deviation from the exponential curve for $V < 150$ mv is likely to be caused by space charge recombination current, possibly at the edge of the diode. This deviation disappeared after about 1 minute under high forward bias, and reappeared after 1 minute under high reverse bias. Note that Au-GaAs diodes are similar to Au-Si diodes in the value of n, indicating that this type of non-ideality is determined by the metal. It is expected that all the current in the region of $n = 1.1$ is hot electron current. The best way to test this point is to examine the dependence of the emitter and collector currents of a GaAs-Au-Si triode upon the emitter-base voltage.

GaAs emitter tripods were prepared using 0.05 ohm-cm n-type material. A triode was fabricated by pressing one of these tripods against a 200Å gold film which had been evaporated onto a 1.4 ohm-cm n-type Si collector, as indicated in Figure 20. The emitter and collector currents are shown in Figure 24 as a function of emitter-base voltage with $V_{cb} = 0$.

Two sets of emitter and collector current curves are shown. The set represented by open circles is the data taken on the device as originally fabricated. The gain (α) is 10^{-6} rising to 10^{-3} at high emitter currents. After judicious jarring of the emitter, the gain increased to 10^{-1} at high cur-

rents. This data is shown by solid circles. It can be seen that although the collector current has changed by orders of magnitude, the emitter current is changed only slightly.

The reason for the very low value of α, and its change with mechanical shock, is unknown. In attempting to explain the characteristics, it is useful to start with an estimate of the contact area of the emitter. By extrapolating the exponential portion of the emitter current to higher currents, we estimate the emitter spreading resistance at a current level of 10^{-5}A to be about 2.5×10^{4} ohms. This leads to a contact diameter of about 100Å. While this estimate is very approximate, it certainly suggests firstly, that surface currents around the contact edge can dominate the normal area currents; and secondly, that the emitter is operating at very high current densities for $I_e > 10^{-6}$A. The low value of α and its variability might, therefore, be the result of surface currents which depend on contact area and location. The value of $n = 1.5$ which characterizes the collector current in the final state, shown in Figure 24, is unexpected since the collector current should consist only of hot electron current and should, therefore, be characterized by $n = 1.0$ or by $n = 1.1$, as shown for the Au-GaAs diode in Figure 23. Note, however, that in the voltage region where data could be obtained on the collector current, the emitter was operating at a current density greater than 10^{5}A/cm^{2}, using the estimated contact diameter of 100Å.

The ideal diode equation does not apply at this high current density.

Figure 25 shows data from another GaAs-Au-Si triode structure. The current transfer ratio (α) rises from 2×10^{-2} to 0.3 at the highest currents measured. In this unit, the collector current is not proportional to $\exp(qV/nkT)$. The gold base thickness for this sample was 100Å. Using an estimated range of 600Å for 1 eV hot electrons in gold, the current transfer ratio should be approximately 0.85 instead of the maximum value of 0.3 observed. Again, the emitter spreading resistance is very high, being about 10^6 ohms at V_{EB} = 0.8 volts and decreasing to about 10^5 ohms at V_B = 2.4 volts. Triodes will be made using more heavily doped GaAs in an attempt to reduce this emitter resistance and allow more easily interpretable data to be obtained.

An oscilloscope tracing of the collector characteristic of another GaAs-Au-Si triode with point emitter and 200Å Au base in Figure 26. The first trace (I_B = 0) is sloped upward because of collector-base leakage. For base drive between 1 and 10 μa, the β is constant. At V_{CE} = 1.6v, the grounded emitter gain β = 3 and α = 0.7 for the first increment. The limiting value of α, due to base transport efficiency, should be $e^{-t/L}$ = 0.72, so it is clear that no other major gain limiting mechanisms exist on this device. The reason for the rapidly decreasing value of β at high currents is not known. This triode did not remain in this high gain condition for a long

enough time to permit detailed measurement of the voltage dependence of the emitter and collector currents.

One of the major motivations for building and analyzing point emitter triodes is that we might be able to determine the range of hot electrons in the metal base by varying the base width and observing the variation of α. Since the triode built up to this time show α varying with current and with mechanical shock, and since the showed no regular dependence on base width, the range has not been determined. Accordingly, the major effort on triode in the next interval will be on the type which uses a deposited, polycrystalline emitter or collector.

IV. PERSONNEL

Individuals who contributed to the contract activity in this report period are:

M. M. Atalla

R. W. Soshea

R. C. Lucas

D. A. Reid

V. M. Dowler

V. VISITORS, CONFERENCES, TRAVEL, PUBLICATIONS

Visitors

Mr. R. F. Cornelissen of AFCRL visited this laboratory on January 30, 1963 to discuss progress of this contract with Drs. M. M. Atalla and R. W. Soshea.

Conferences

No conferences were attended during this report period.

Travel

There was no travel during this report period.

Publications

During this report period, a paper entitled "Hot Carrier Triodes With Thin-Film Metal Base", authored by M. M. Atalla and R. W. Soshea, was accepted for publication in Solid State Electronics.

FIGURE CAPTIONS

1. Current-voltage characteristic of a Au-Si barrier.
2. Reverse current-voltage characteristic of a Au-Si barrier compared with theoretical curves for the image force barrier lowering effect.
3. Electron energy diagram of a reverse biased Au-Si barrier.
4. Capacity-voltage characteristic of Au-Si barrier at several temperatures.
5. Current-voltage characteristic of Au-Si at 22°C.
6. Current-voltage characteristic of Au-Si at 43.7°C.
7. Current-voltage characteristic of Au-Si at 70.5°C.
8. Current-voltage characteristic of Au-Si at 100.6°C.
9. Temperature dependence of the saturation current. This gives a thermal activation energy of 0.799 eV.
10. Current-voltage characteristic of a Pt-Si barrier. Curvature at high currents is due to series resistance.
11. Capacity-voltage characteristic of a Pt-Si barrier.
12. Current-voltage characteristic of a Pd-Si barrier.
13. Capacity-voltage characteristic of a Pd-Si barrier.
14. Current-voltage characteristic of a Ag-Si barrier.
15. Capacity-voltage characteristic of a Ag-Si barrier.
16. Current-voltage characteristic of a Cu-Si barrier.
17. Capacity-voltage characteristic of a Cu-Si barrier.
18. Current-voltage characteristic of a Ni-Si barrier.
19. Dependence of saturation current density on internal barrier height for several metal-Si contacts.
20. Typical triode structure.
21. Collector characteristics of typical triode with silicon collector, 200Å thick gold base and point contact silicon emitter.

FIGURE CAPTIONS (Continued)

22. $1/C^2$-voltage data for gold-GaAs barrier. From the intercept indicated $V_o = 0.89$, the corresponding barrier height $V_b = 0.916$, the internal barrier height $V_i = 0.977$ eV.

23. Current-voltage characteristic of barrier of Figure 22.

24. Emitter and collector currents of a triode with a silicon collector, a 200Å gold film and gallium arsenide point emitter. Two sets of data are presented: open circles are the original points, the solid points were taken after tapping the structure.

25. Emitter and collector currents of triode with silicon collector, 100Å gold base and gallium arsenide point emitter.

26. Collector characteristic of high gain GaAs-Au-Si triode with 200Å thick gold base and point emitter.

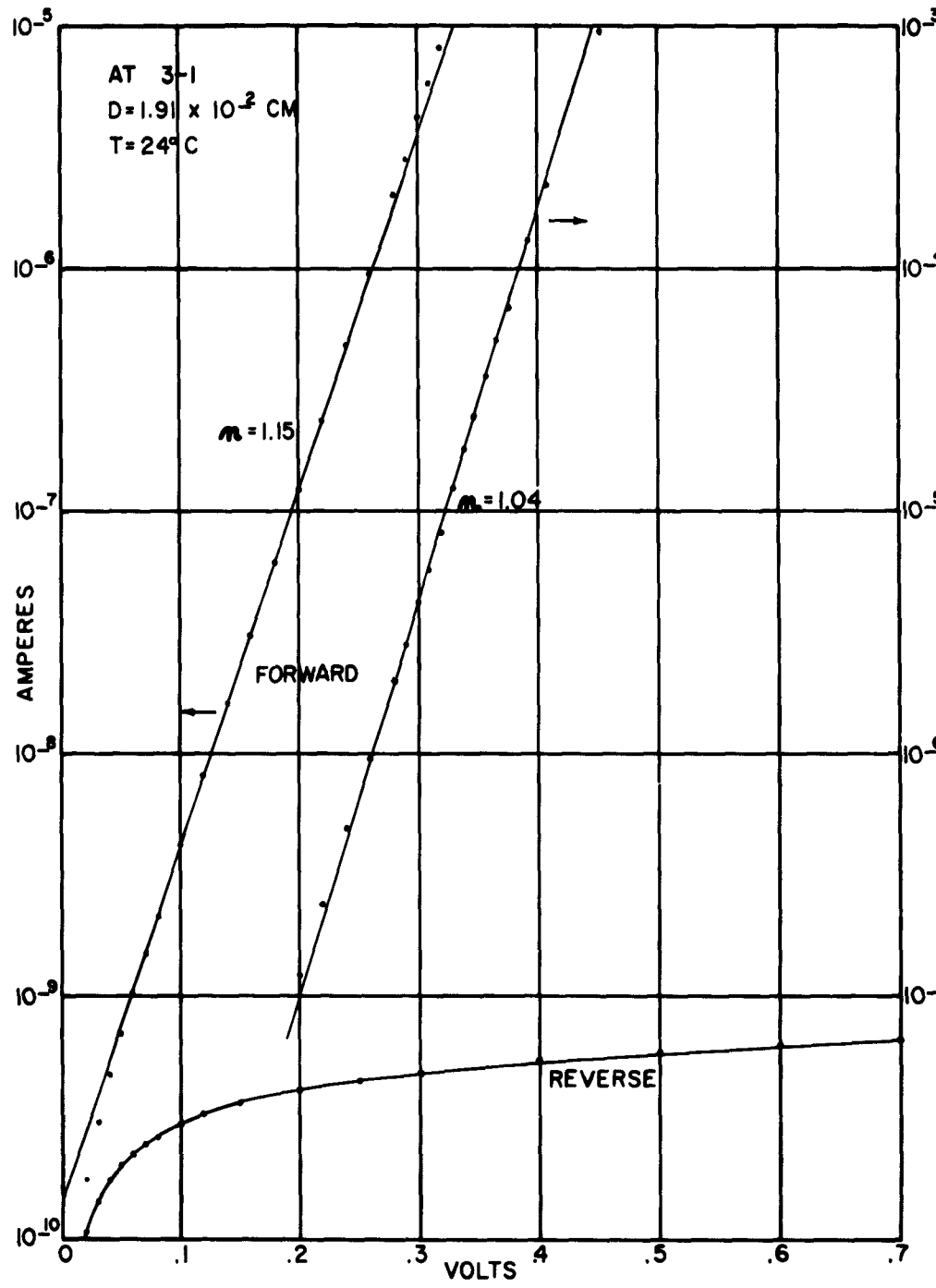
AT 3-1
D = 1.91 x 10⁻² CM
T = 24°C
m = 1.15
m = 1.04
FORWARD
REVERSE
AMPERES
VOLTS
10⁻⁵
10⁻⁶
10⁻⁷
10⁻⁸
10⁻⁹
10⁻¹⁰
10⁻³
10⁻⁴
10⁻⁵
10⁻⁶
10⁻⁷
0
.1
.2
.3
.4
.5
.6
.7

Figure 1

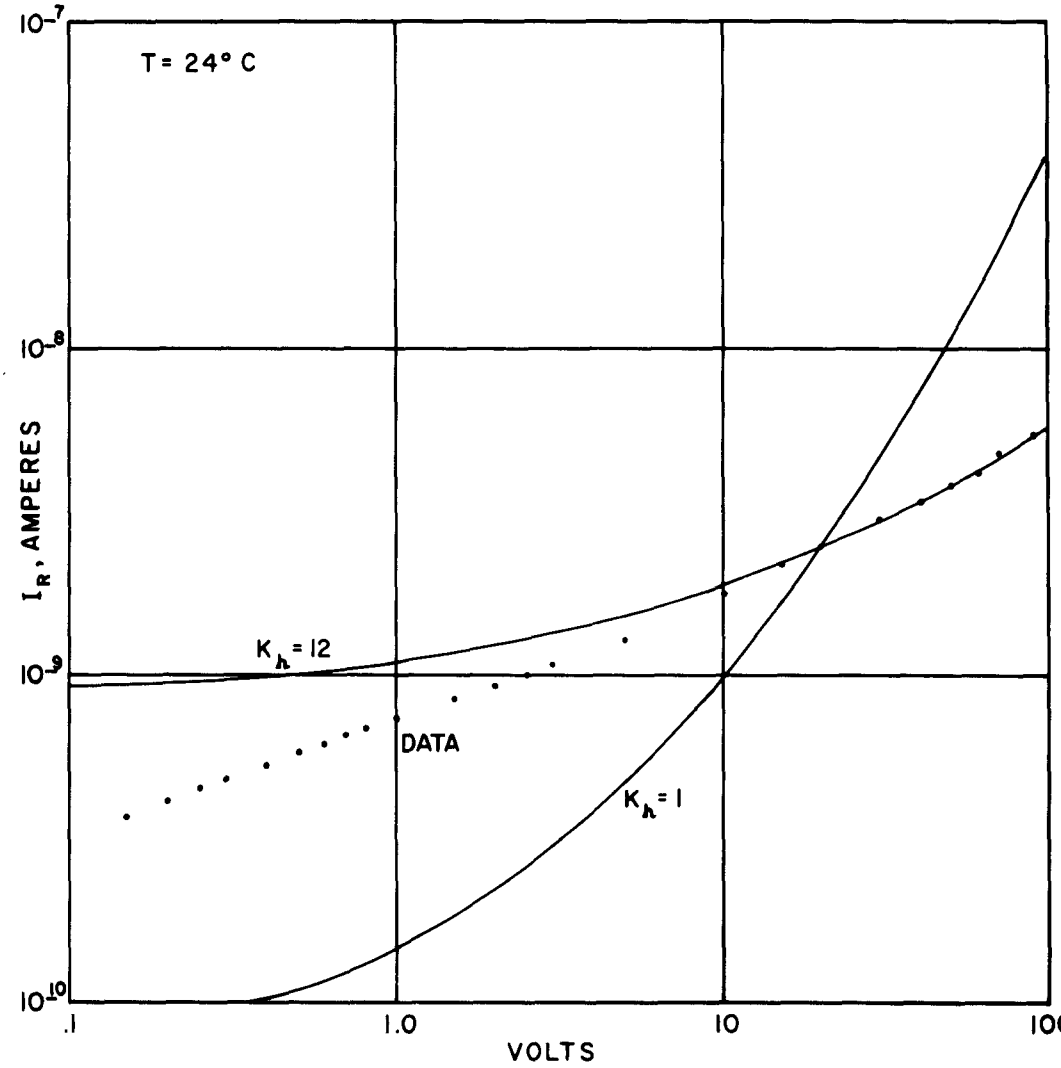
T = 24° C
10^{-7}
10^{-8}
10^{-9}
10^{-10}
I_R, AMPERES
K_h = 12
DATA
K_h = 1
.1
1.0
10
100
VOLTS

Figure 2

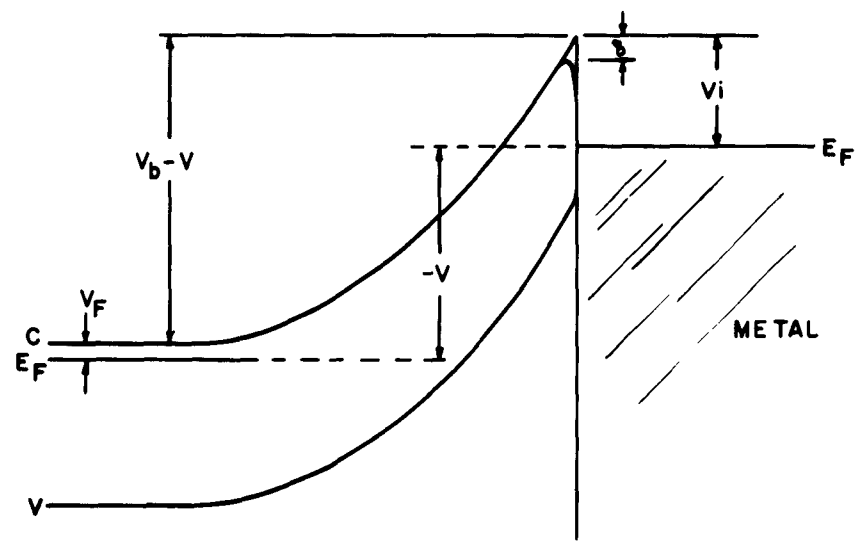

Figure 3

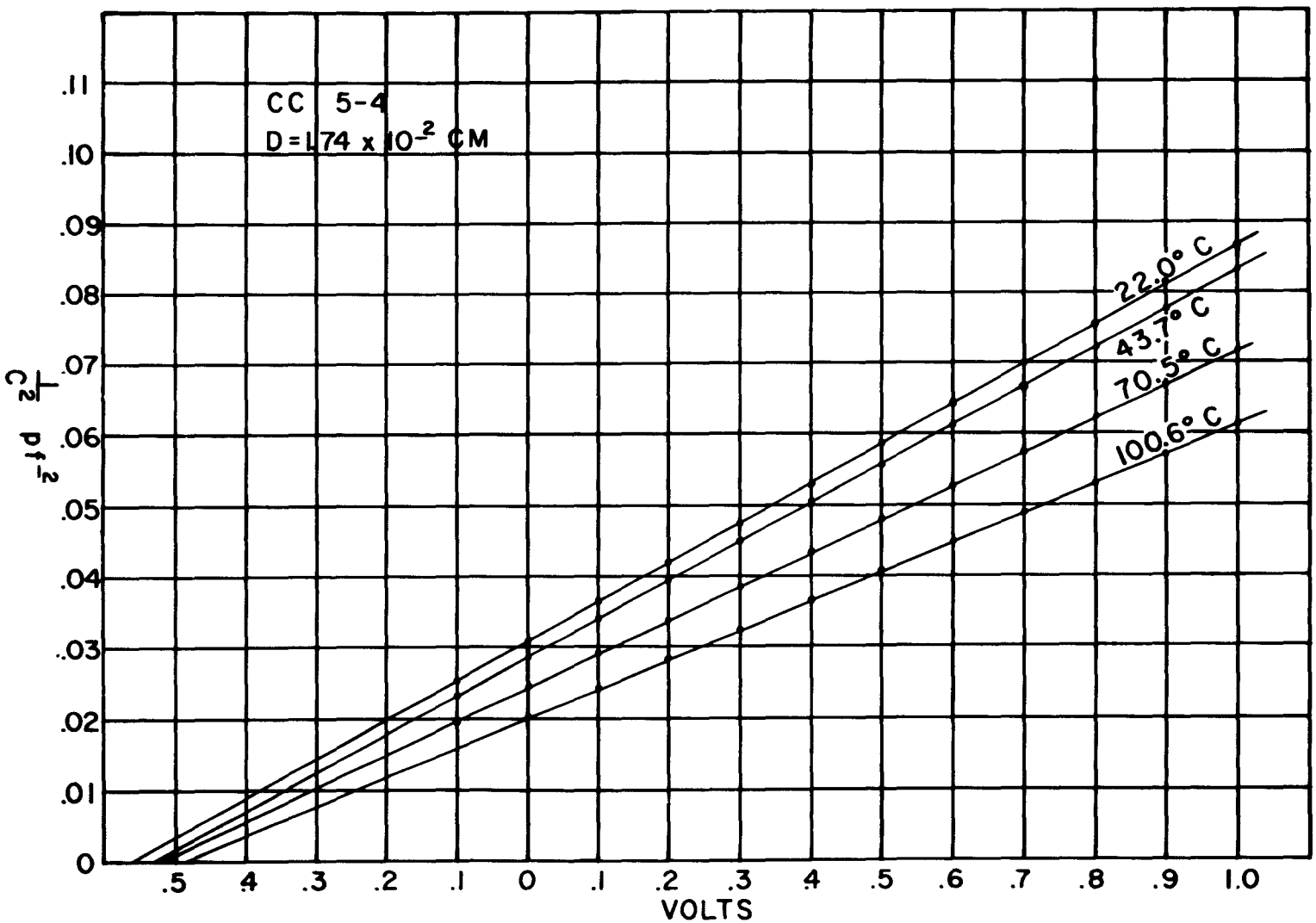
CC 5-4
D = 1.74 x 10⁻² CM
22.0° C
43.7° C
70.5° C
100.6° C
C²/pf²
.11
.10
.09
.08
.07
.06
.05
.04
.03
.02
.01
0
.5 .4 .3 .2 .1 0 .1 .2 .3 .4 .5 .6 .7 .8 .9 1.0
VOLTS

Figure 4

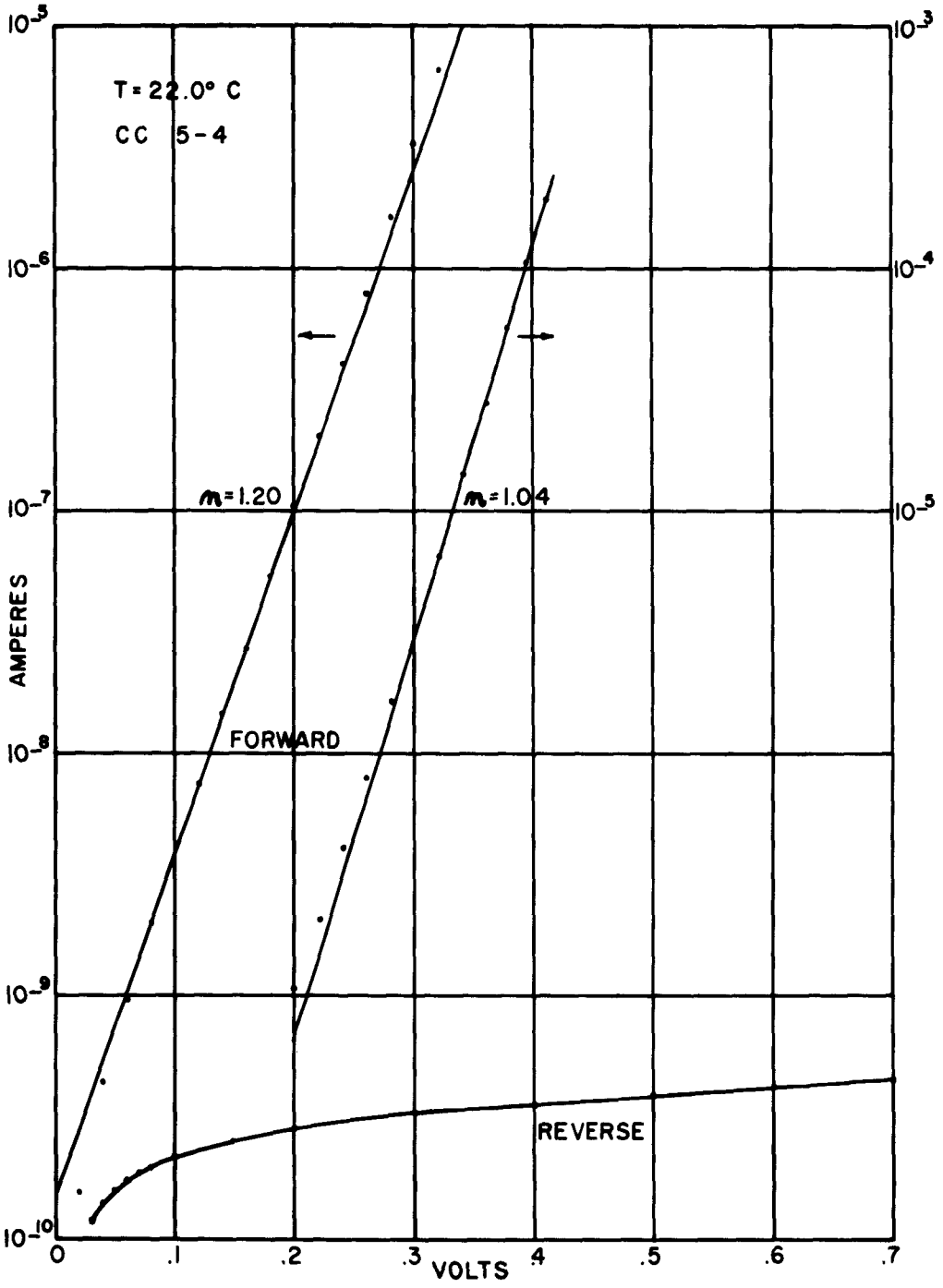
T = 22.0° C
CC 5-4
n = 1.20
n = 1.04
FORWARD
REVERSE
AMPERES
VOLTS
10^-5
10^-6
10^-7
10^-8
10^-9
10^-10
10^-3
10^-4
10^-5
0
.1
.2
.3
.4
.5
.6
.7

Figure 5

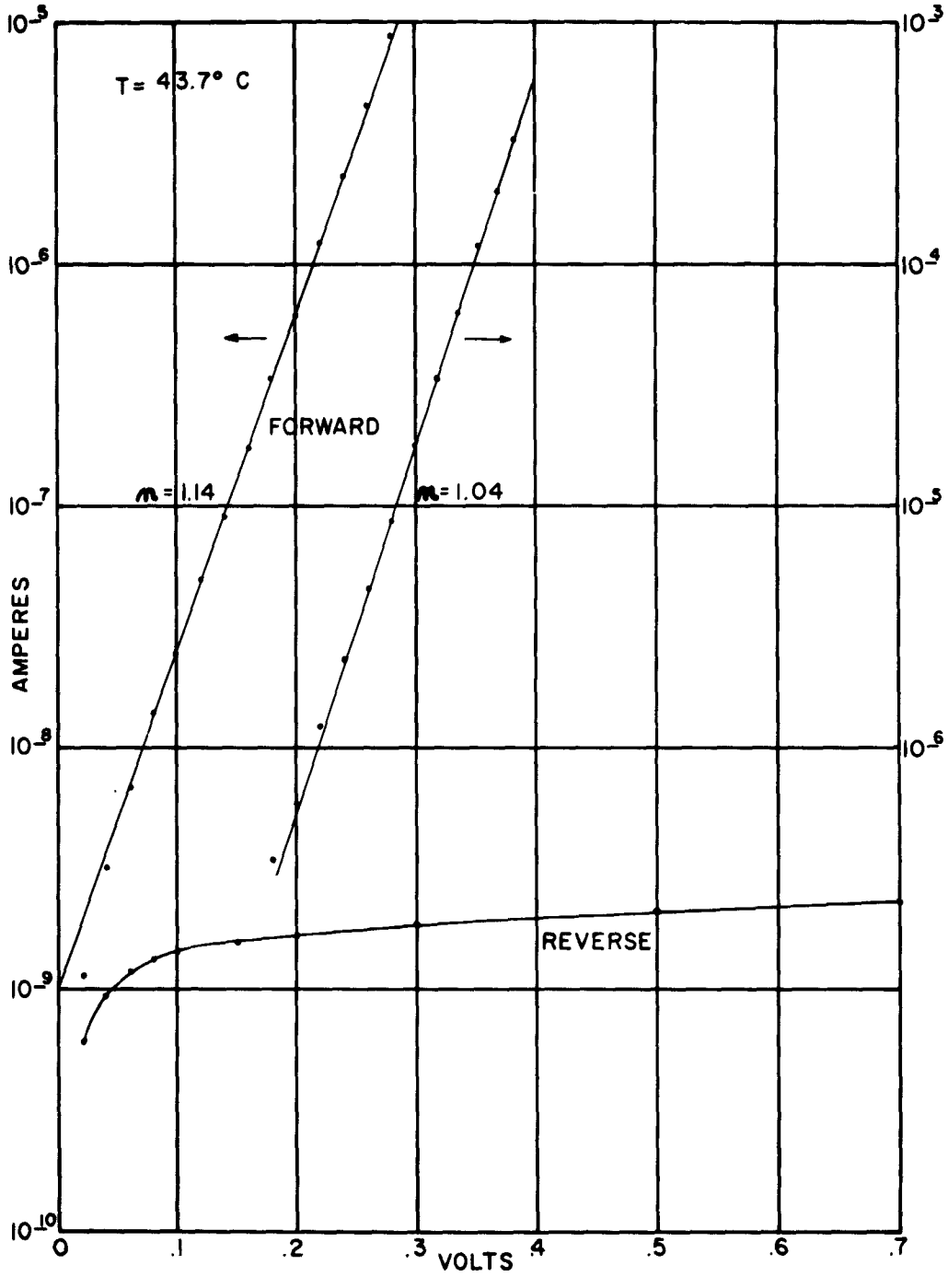
T= 43.7° C
FORWARD
REVERSE
m = 1.14
m = 1.04
AMPERES
VOLTS
10⁻⁵
10⁻⁶
10⁻⁷
10⁻⁸
10⁻⁹
10⁻¹⁰
10⁻³
10⁻⁴
10⁻⁵
10⁻⁶
0
.1
.2
.3
.4
.5
.6
.7

Figure 6

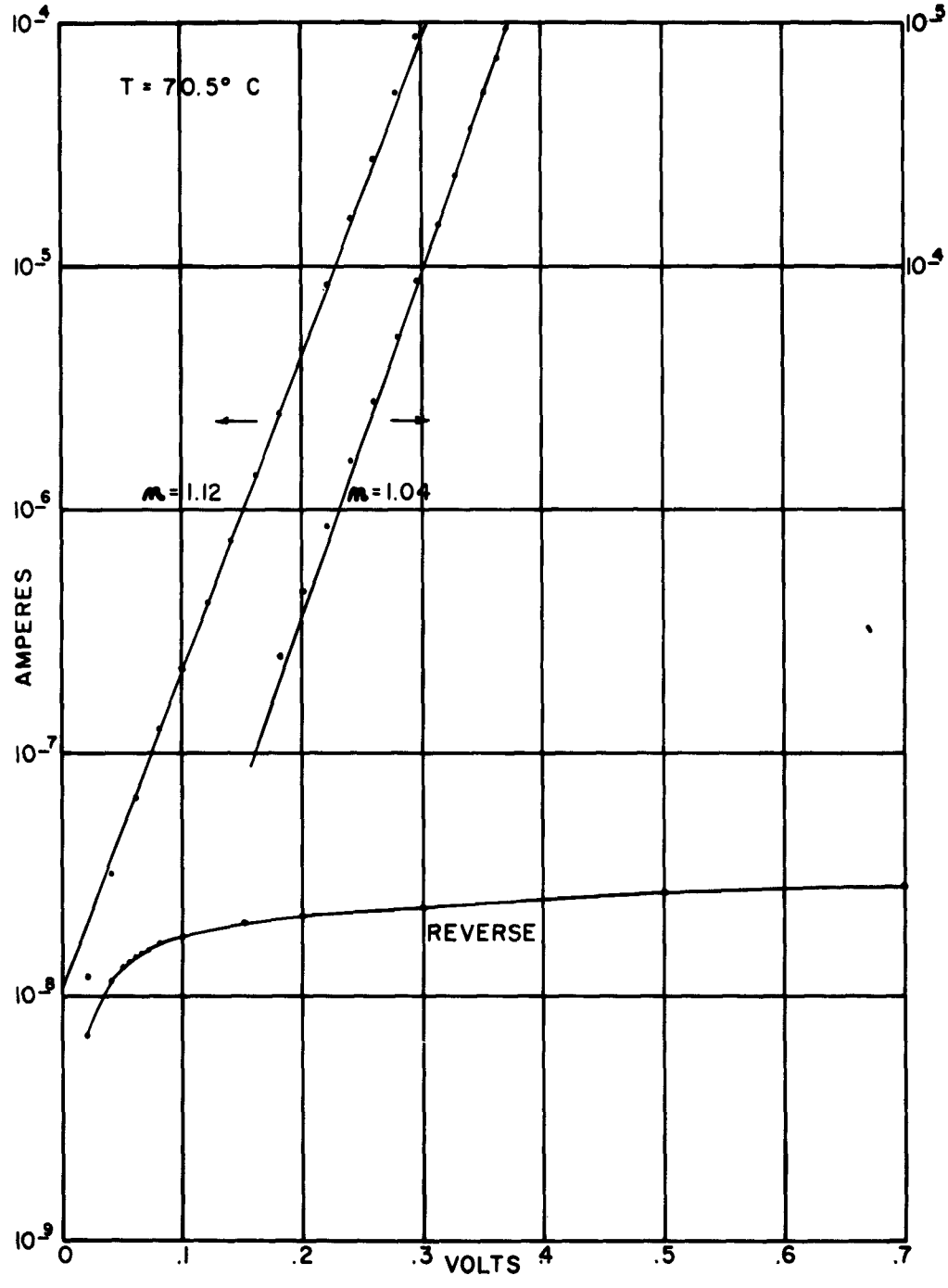
T = 70.5° C
m = 1.12
m = 1.04
REVERSE
AMPERES
VOLTS
10⁻⁴
10⁻⁵
10⁻⁶
10⁻⁷
10⁻⁸
10⁻⁹
0
.1
.2
.3
.4
.5
.6
.7

Figure 7

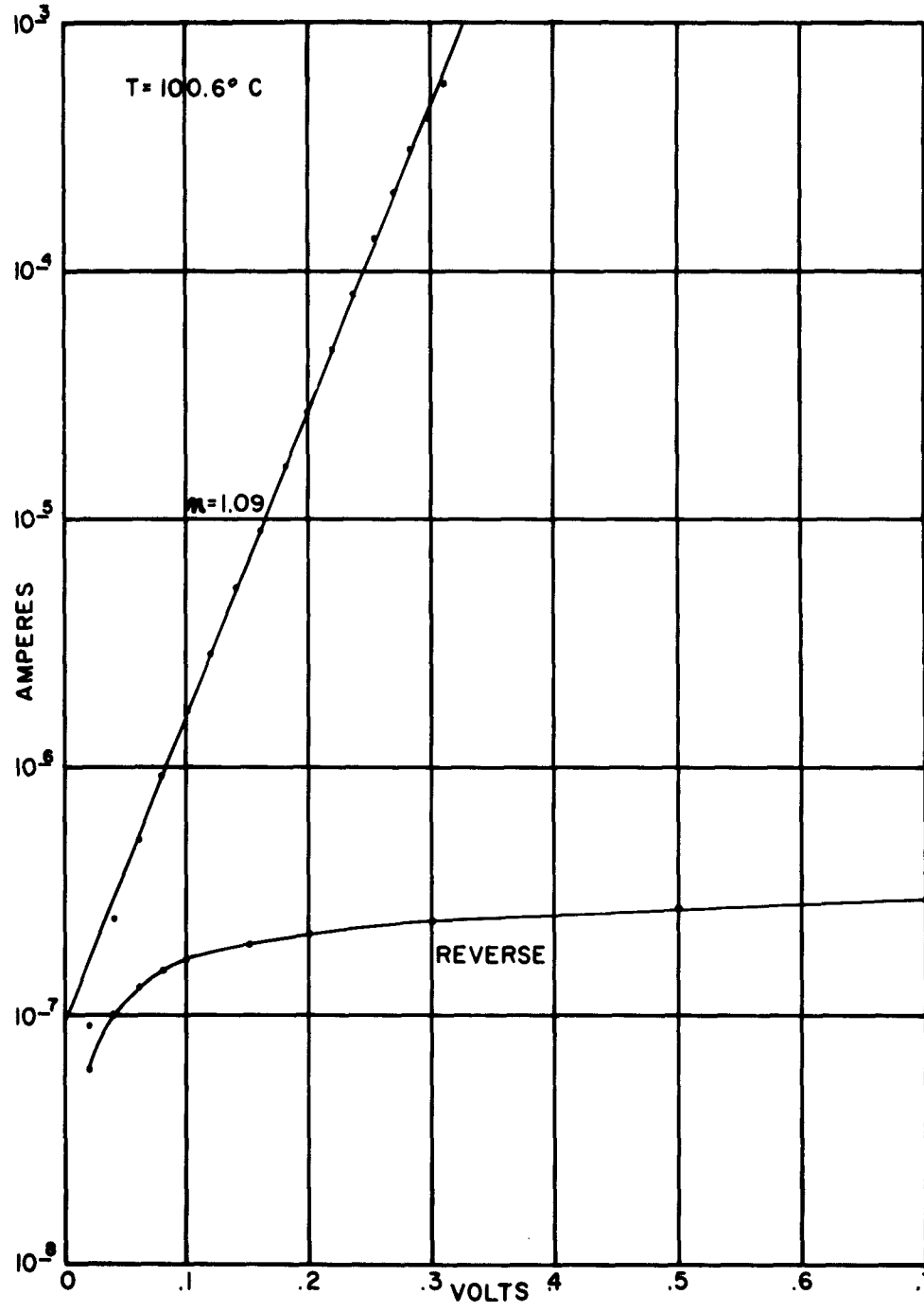
T= 100.6° C
n=1.09
REVERSE
AMPERES
VOLTS
10^{-3}
10^{-4}
10^{-5}
10^{-6}
10^{-7}
10^{-8}
0
.1
.2
.3
.4
.5
.6
.7

Figure 8

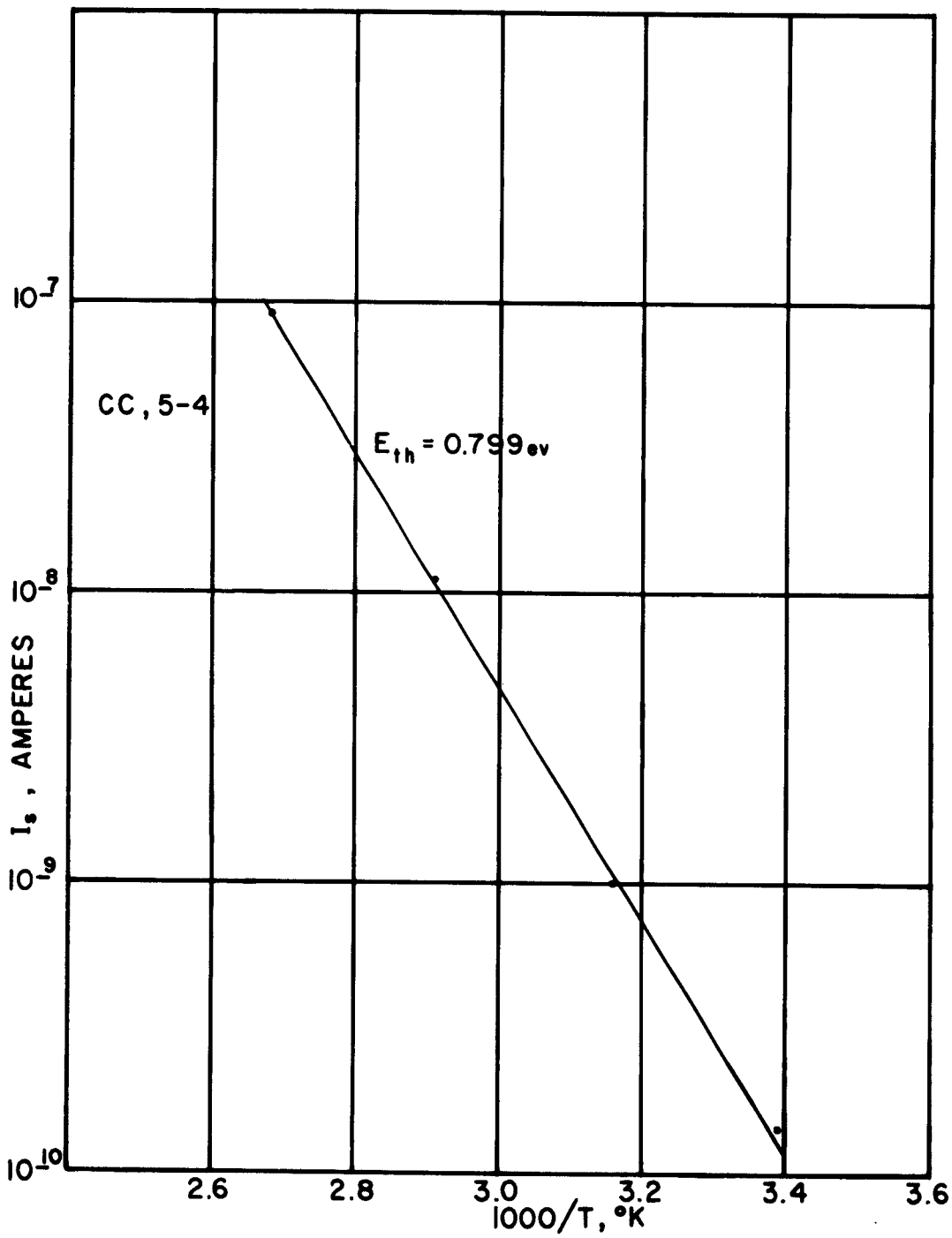
CC, 5-4
E_{th} = 0.799ev
10^{-7}
10^{-8}
10^{-9}
10^{-10}
I_s, AMPERES
2.6
2.8
3.0
3.2
3.4
3.6
1000/T, °K

Figure 9

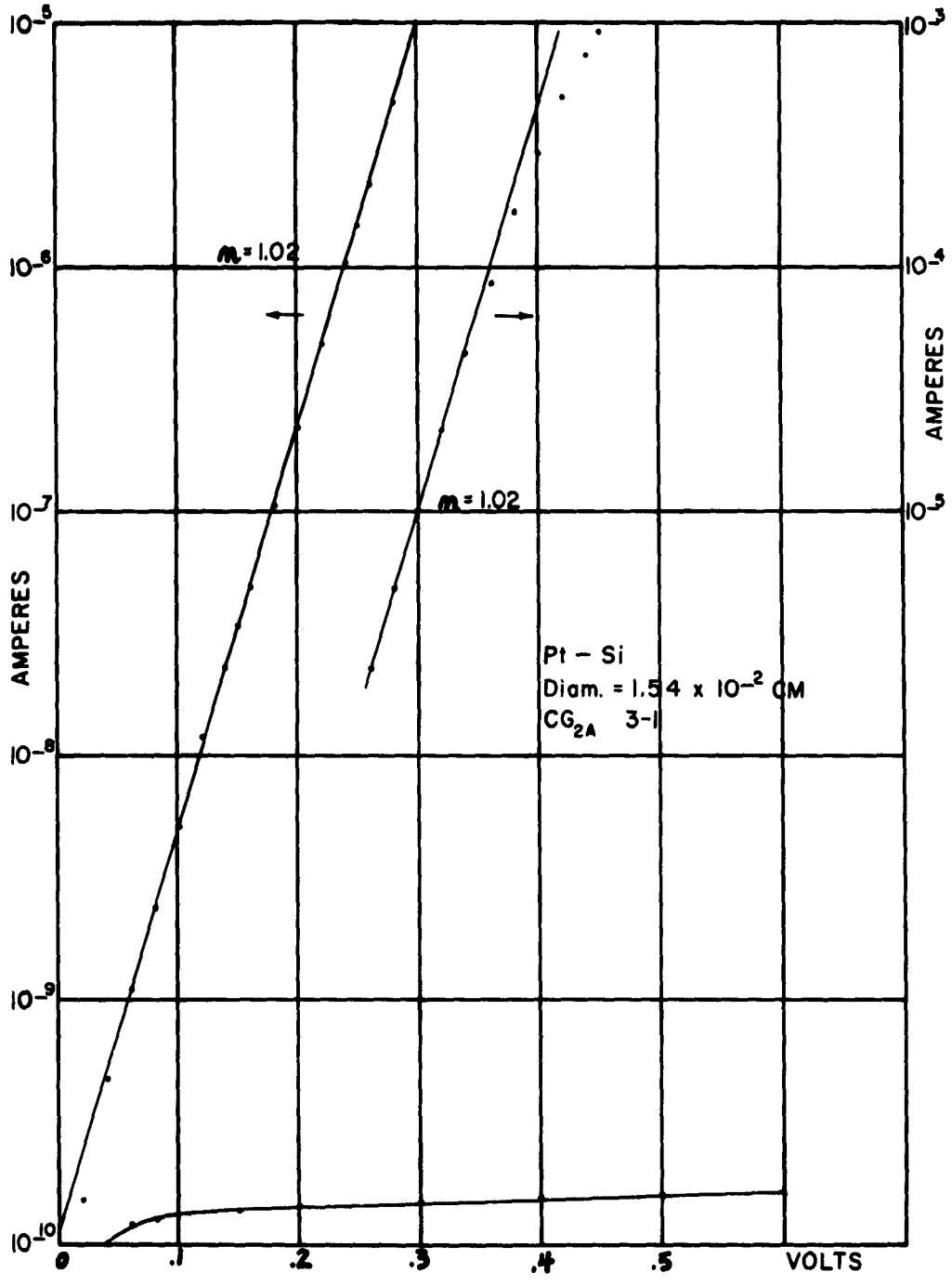
10^{-5}
10^{-6}
10^{-7}
10^{-8}
10^{-9}
10^{-10}
AMPERES
10^{-3}
10^{-4}
10^{-5}
AMPERES
m = 1.02
m = 1.02
Pt – Si
Diam. = 1.54 x 10^{-2} CM
CG_{2A} 3-1
0
.1
.2
.3
.4
.5
VOLTS

Figure 10

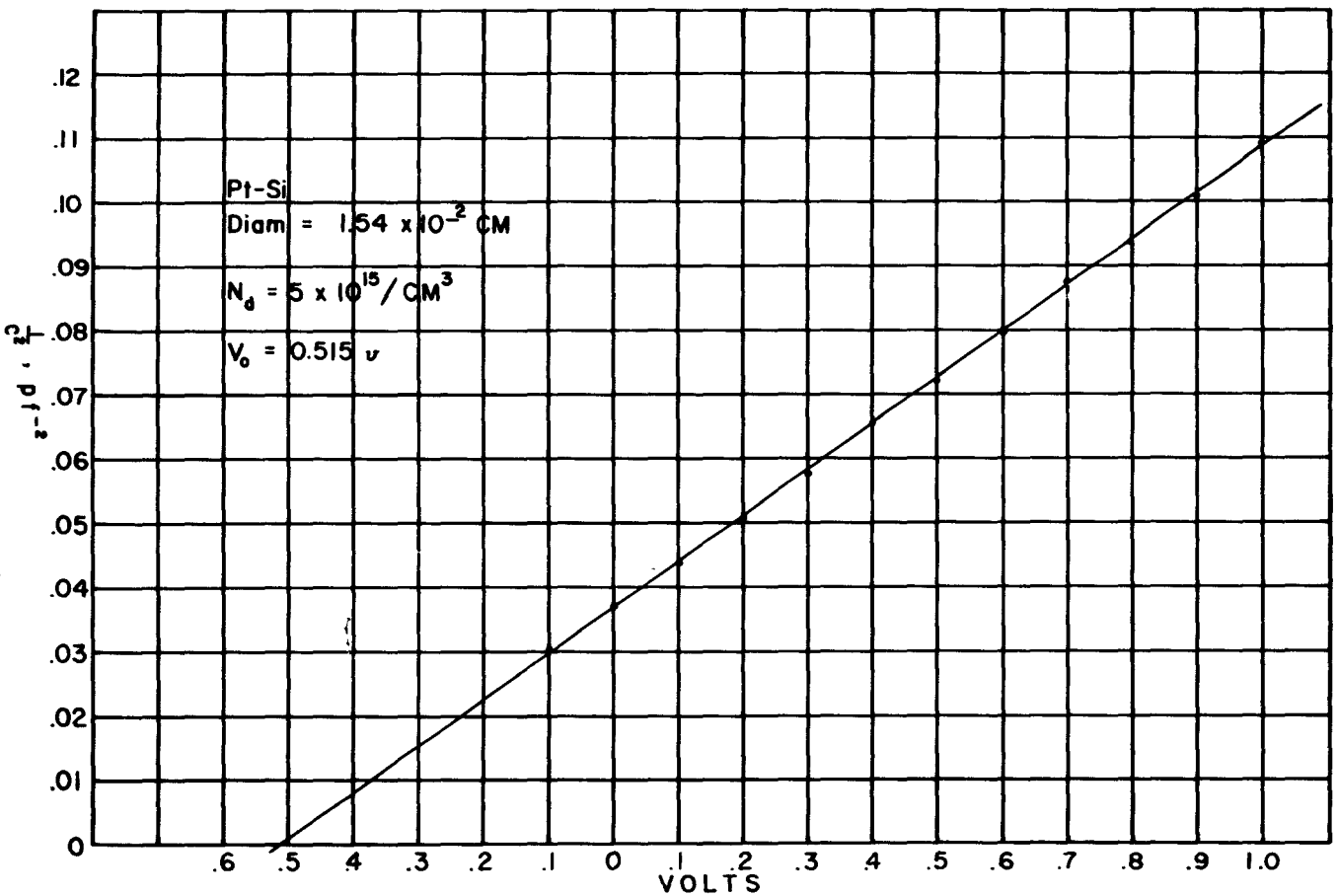
Pt-Si
Diam = 1.54 x10^{-2} CM
N_d = 5 x 10^{15}/CM^3
V_o = 0.515 v
C^{-2}, pf^{-2}
.12
.11
.10
.09
.08
.07
.06
.05
.04
.03
.02
.01
0
.6 .5 .4 .3 .2 .1 0 .1 .2 .3 .4 .5 .6 .7 .8 .9 1.0
VOLTS

Figure 11

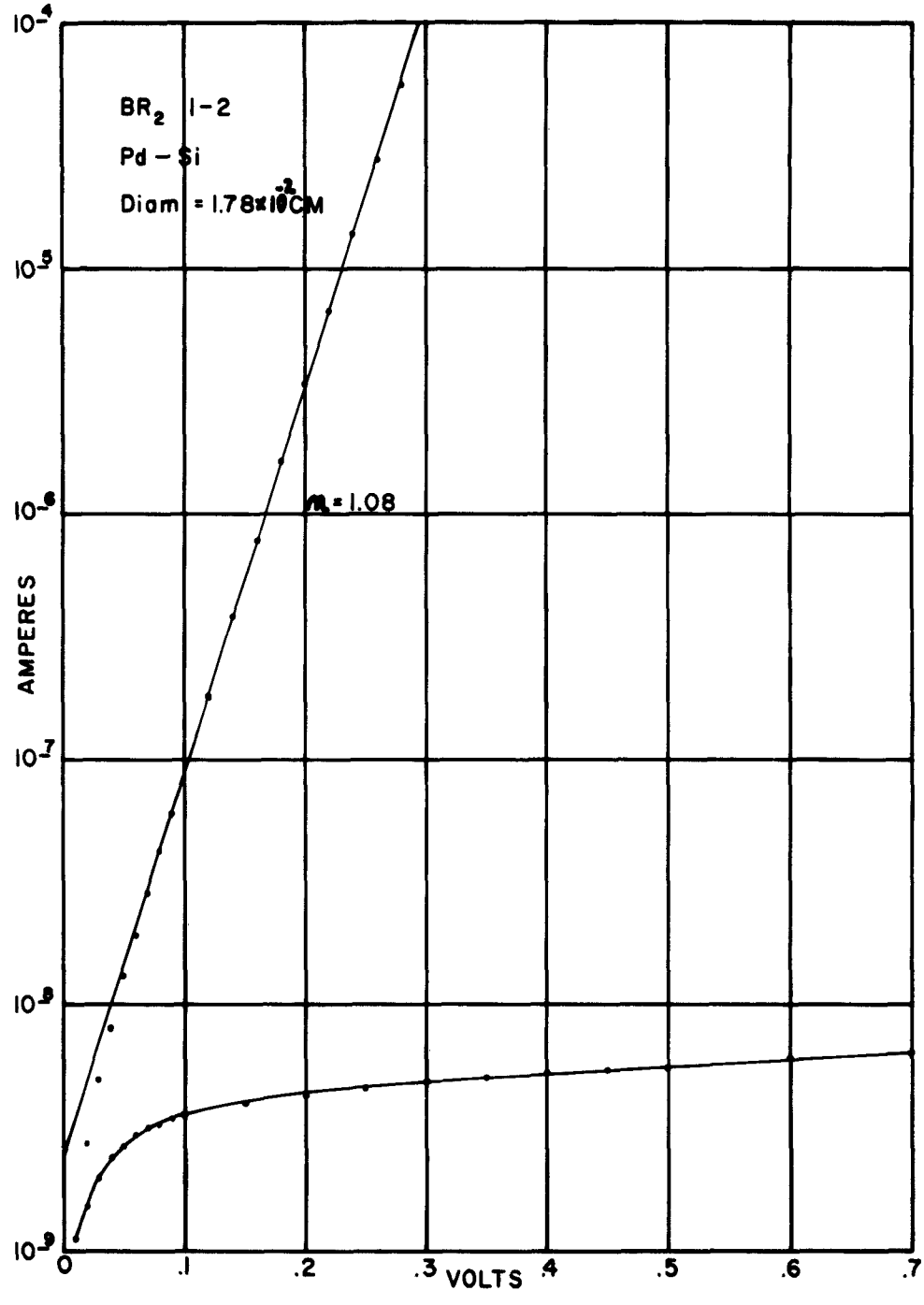
BR_2 1-2
Pd – Si
Diam = 1.78×10⁻²CM
n = 1.08
AMPERES
VOLTS
10⁻⁴
10⁻⁵
10⁻⁶
10⁻⁷
10⁻⁸
10⁻⁹
0
.1
.2
.3
.4
.5
.6
.7

Figure 12

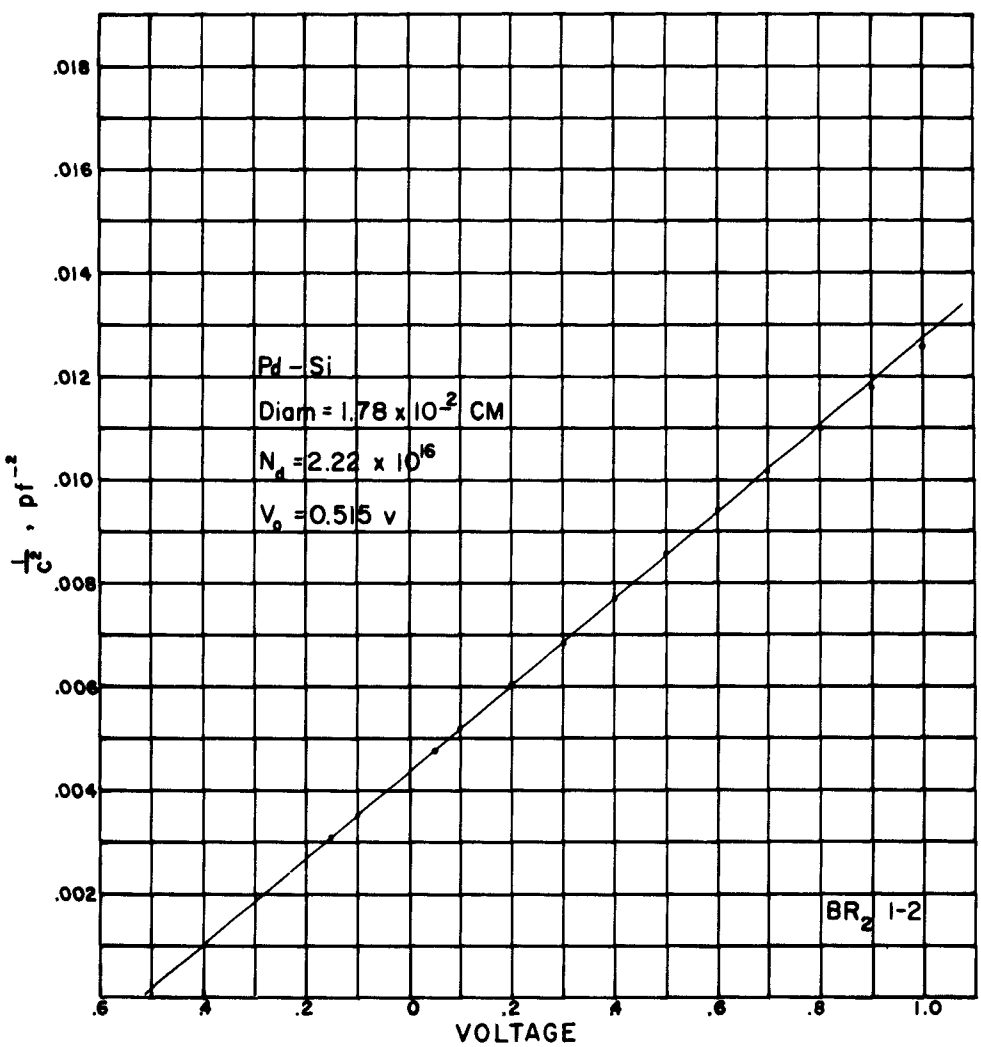
.018
.016
.014
.012
.010
.008
.006
.004
.002
$\frac{1}{C^2}$, pf^{-2}
Pd – Si
Diam = 1.78 x 10^{-2} CM
N_d = 2.22 x 10^{16}
V_o = 0.515 v
BR_2 1-2
.6
.4
.2
0
.2
.4
.6
.8
1.0
VOLTAGE

Figure 13

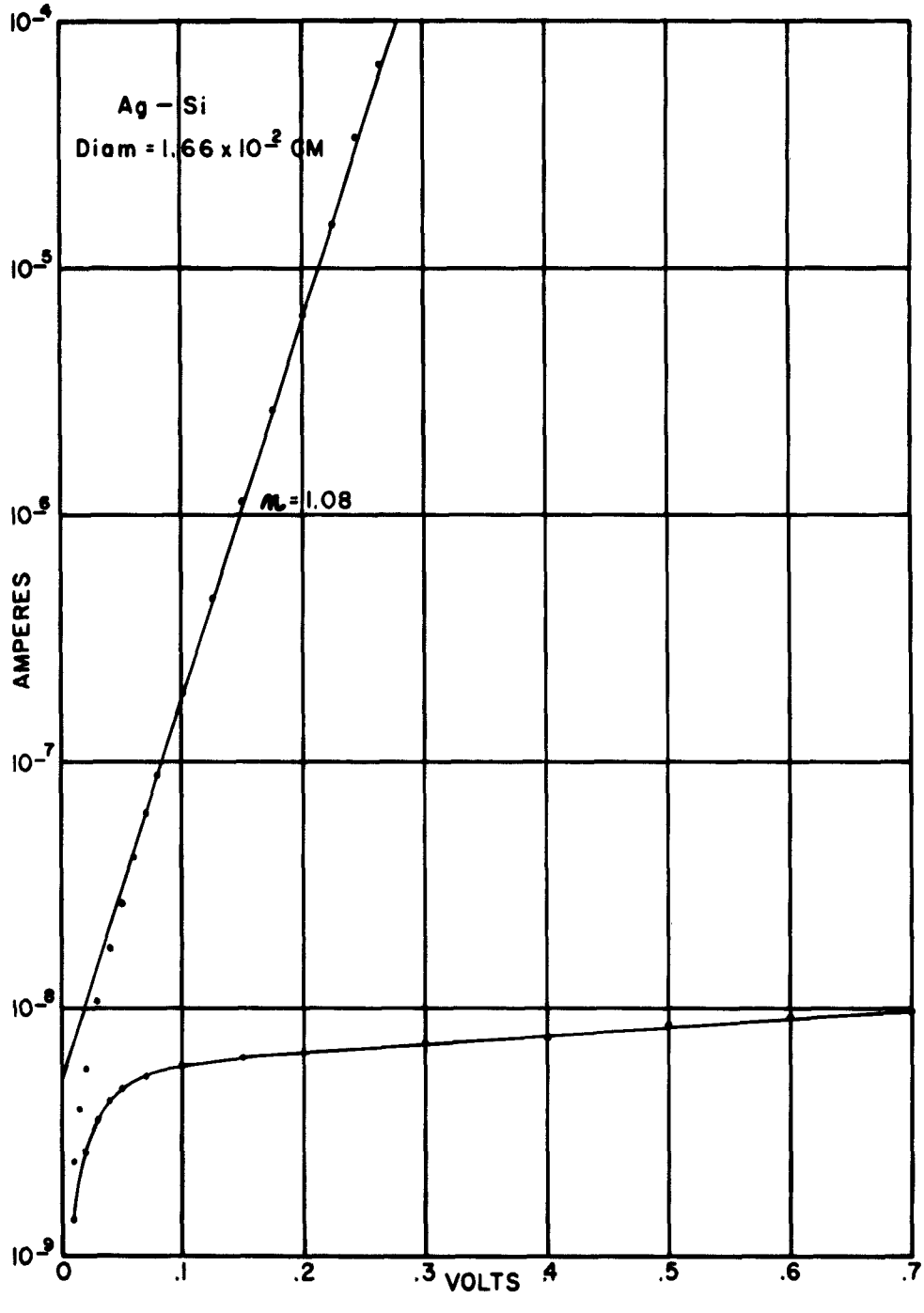
Ag – Si
Diam = 1.66 x 10⁻² CM
n = 1.08
AMPERES
VOLTS
10⁻⁴
10⁻⁵
10⁻⁶
10⁻⁷
10⁻⁸
10⁻⁹
0
.1
.2
.3
.4
.5
.6
.7

Figure 14

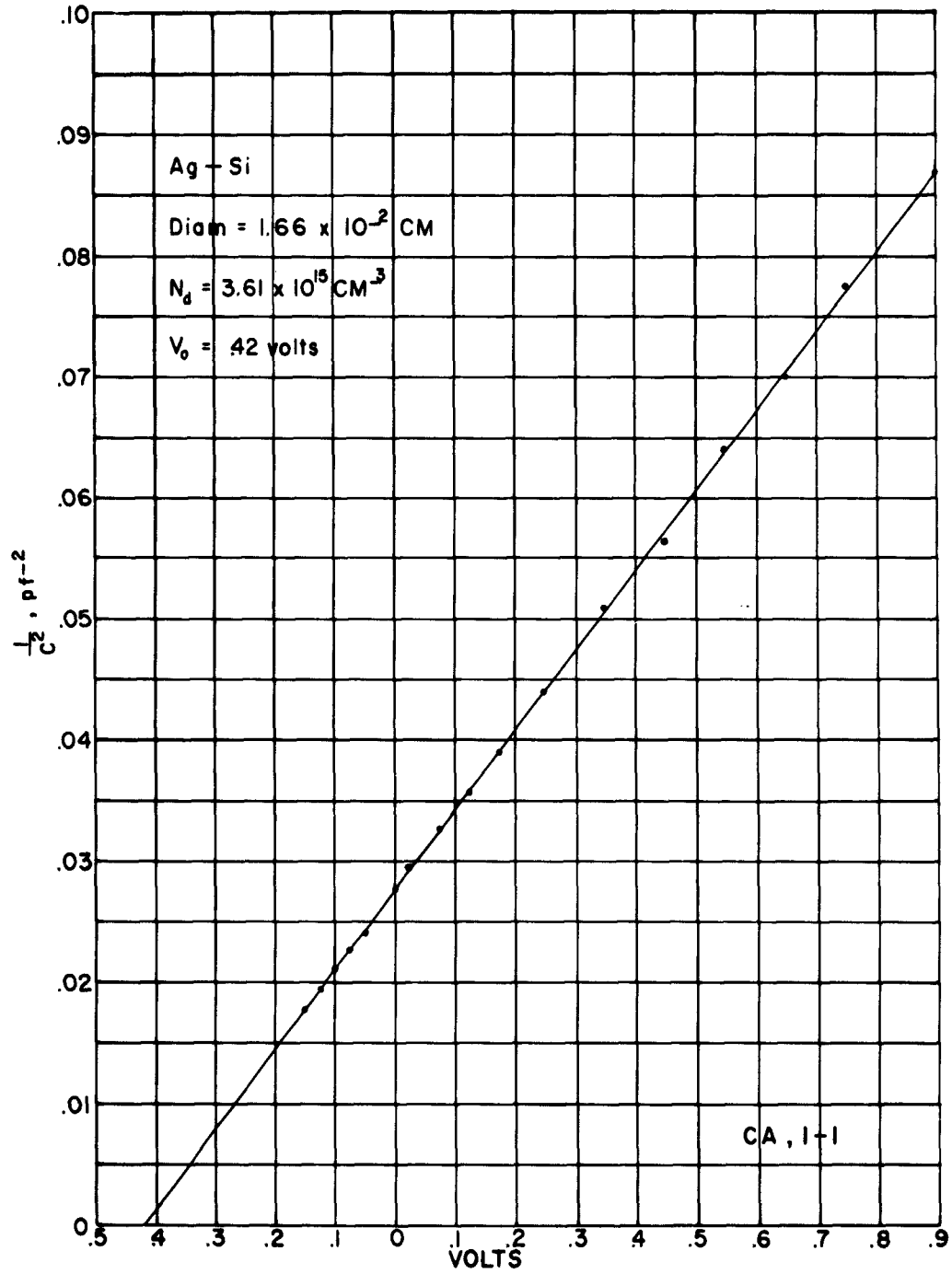
Ag – Si
Diam = 1.66 x 10⁻² CM
N_d = 3.61 x 10¹⁵ CM⁻³
V_o = .42 volts
CA, 1-1
1/C², pf⁻²
VOLTS
.10
.09
.08
.07
.06
.05
.04
.03
.02
.01
0
.5
.4
.3
.2
.1
0
.1
.2
.3
.4
.5
.6
.7
.8
.9

Figure 15

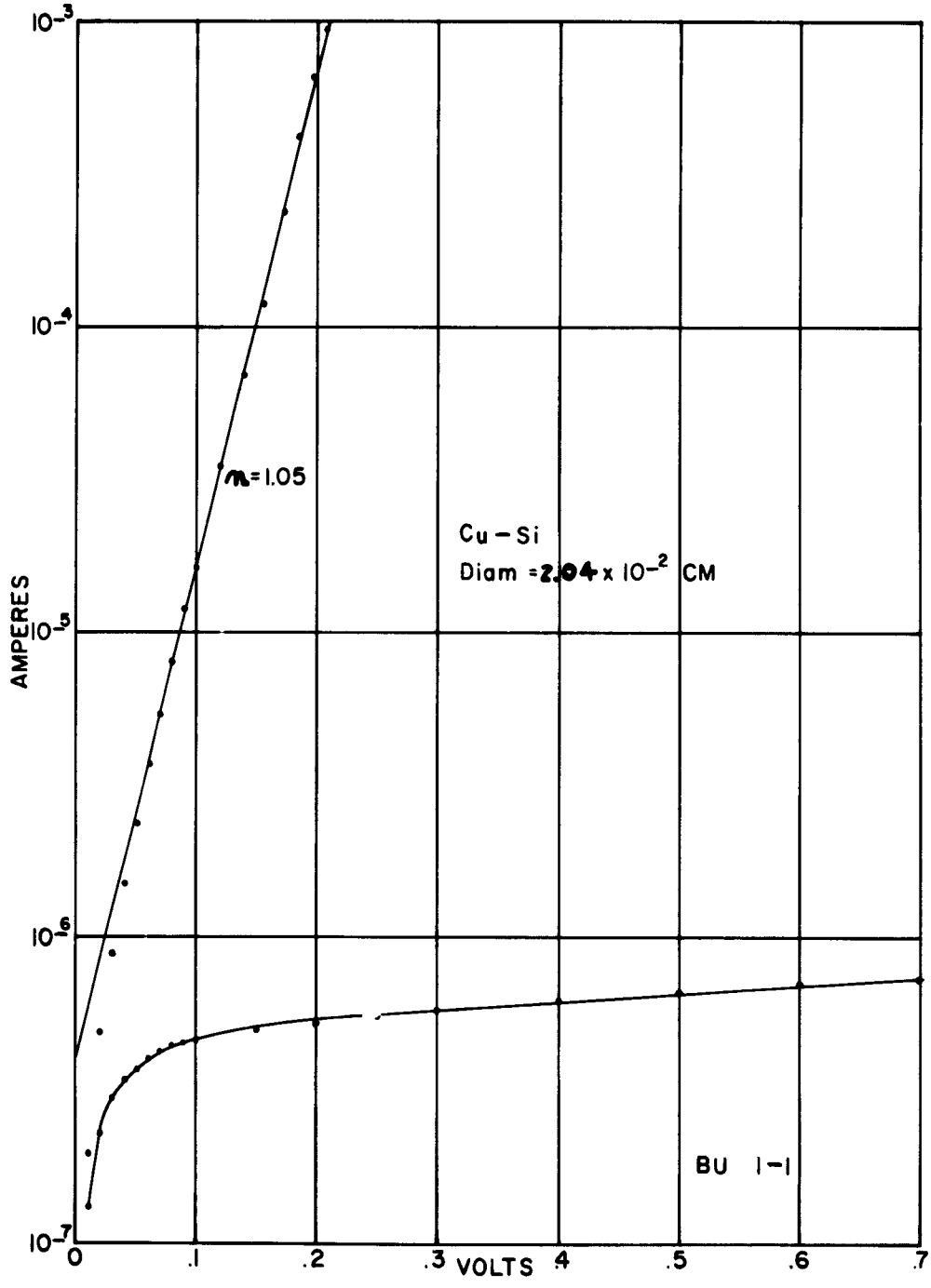
10^{-3}
10^{-4}
10^{-5}
10^{-6}
10^{-7}
AMPERES
n = 1.05
Cu – Si
Diam = 2.04 x 10^{-2} CM
BU 1-1
0
.1
.2
.3
VOLTS
.4
.5
.6
.7

Figure 16

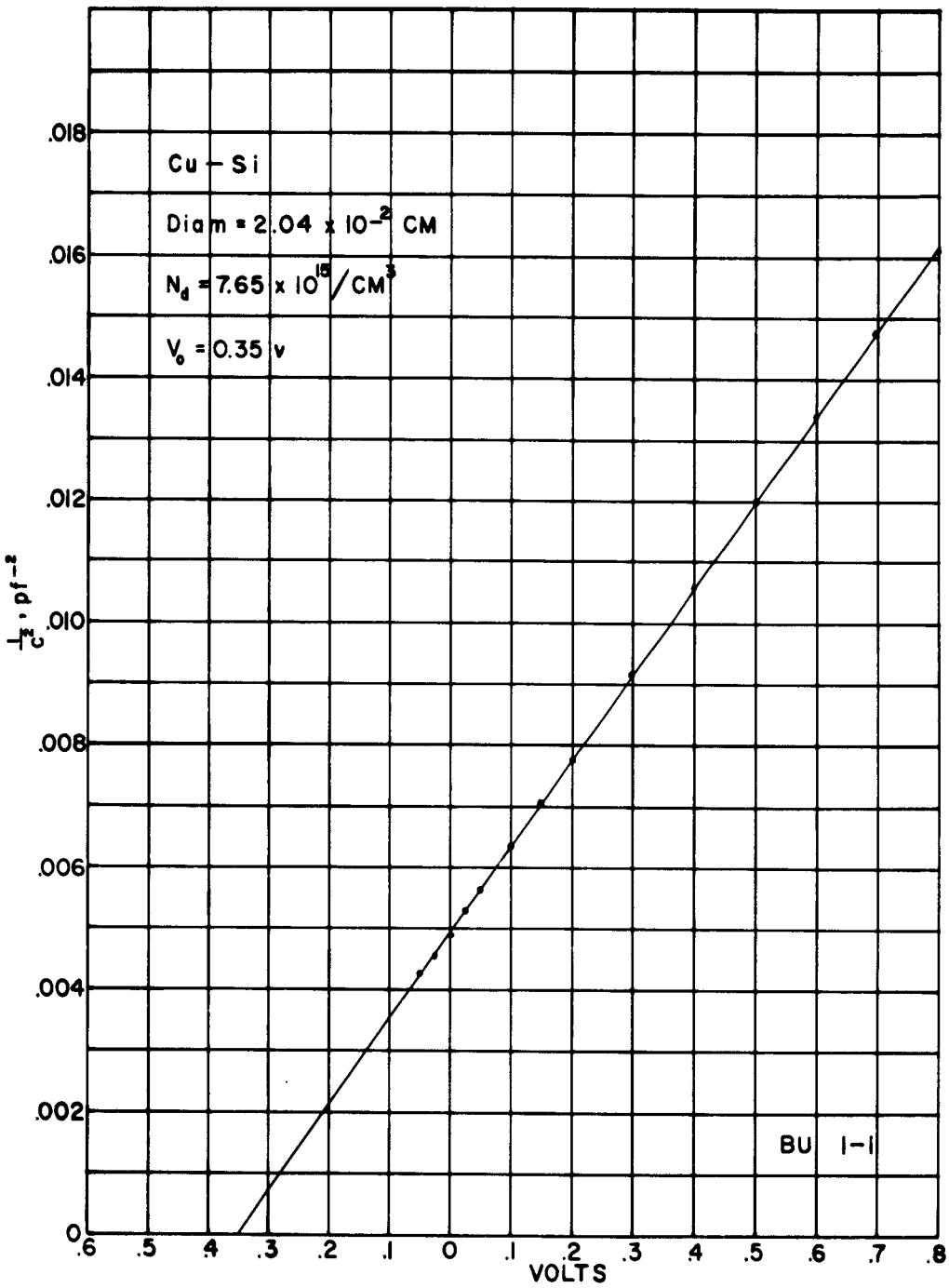
Cu – Si
Diam = 2.04 x 10⁻² CM
N_d = 7.65 x 10¹⁵/CM³
V_0 = 0.35 v
BU 1-1
1/C², pf⁻²
VOLTS
0
.002
.004
.006
.008
.010
.012
.014
.016
.018
.6
.5
.4
.3
.2
.1
0
.1
.2
.3
.4
.5
.6
.7
.8

Figure 17

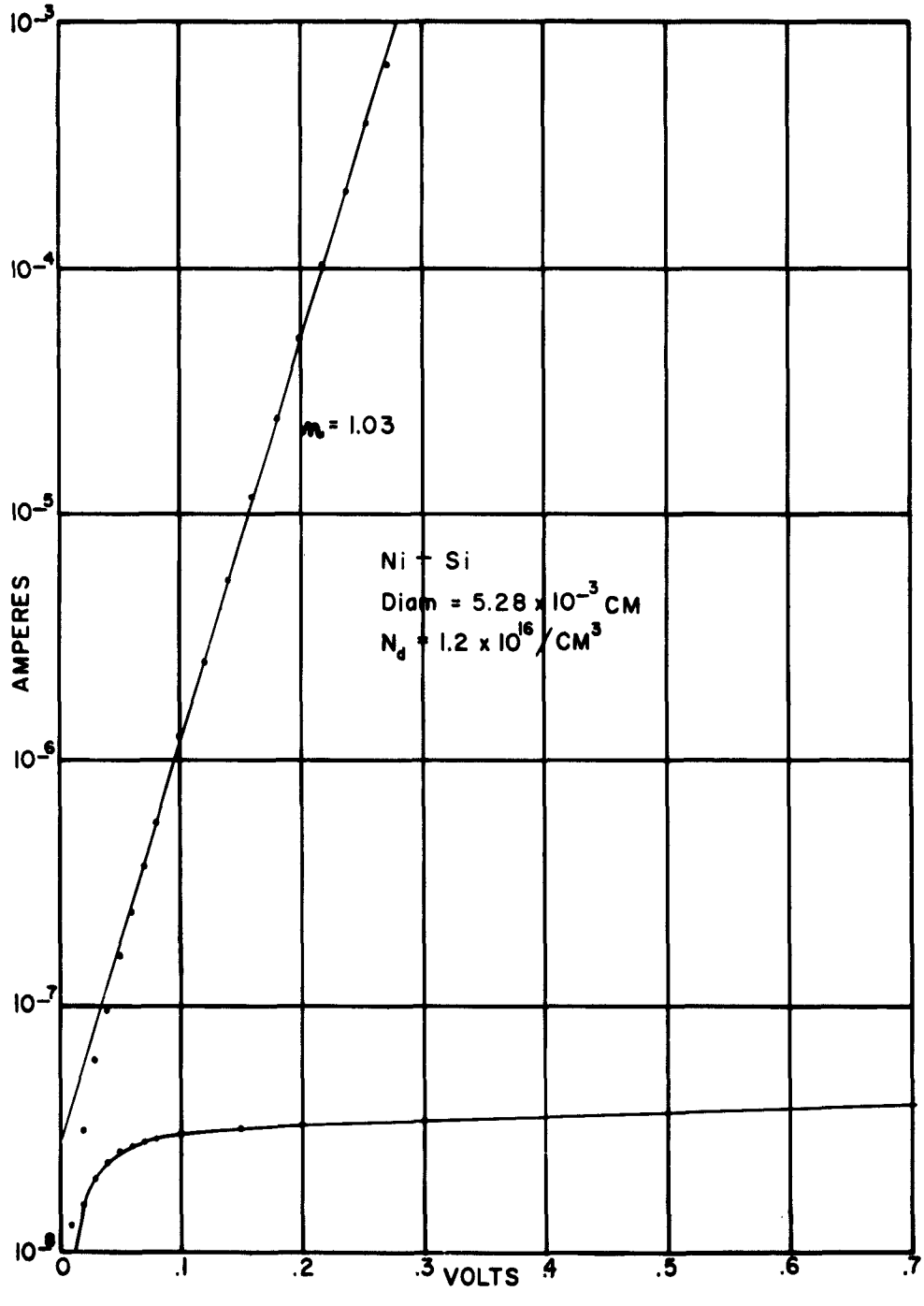
10^{-3}
10^{-4}
10^{-5}
10^{-6}
10^{-7}
10^{-8}
AMPERES
n = 1.03
Ni - Si
Diam = 5.28×10^{-3} CM
$N_d = 1.2 \times 10^{16}$ / CM^3
0
.1
.2
.3
VOLTS
.4
.5
.6
.7

Figure 18

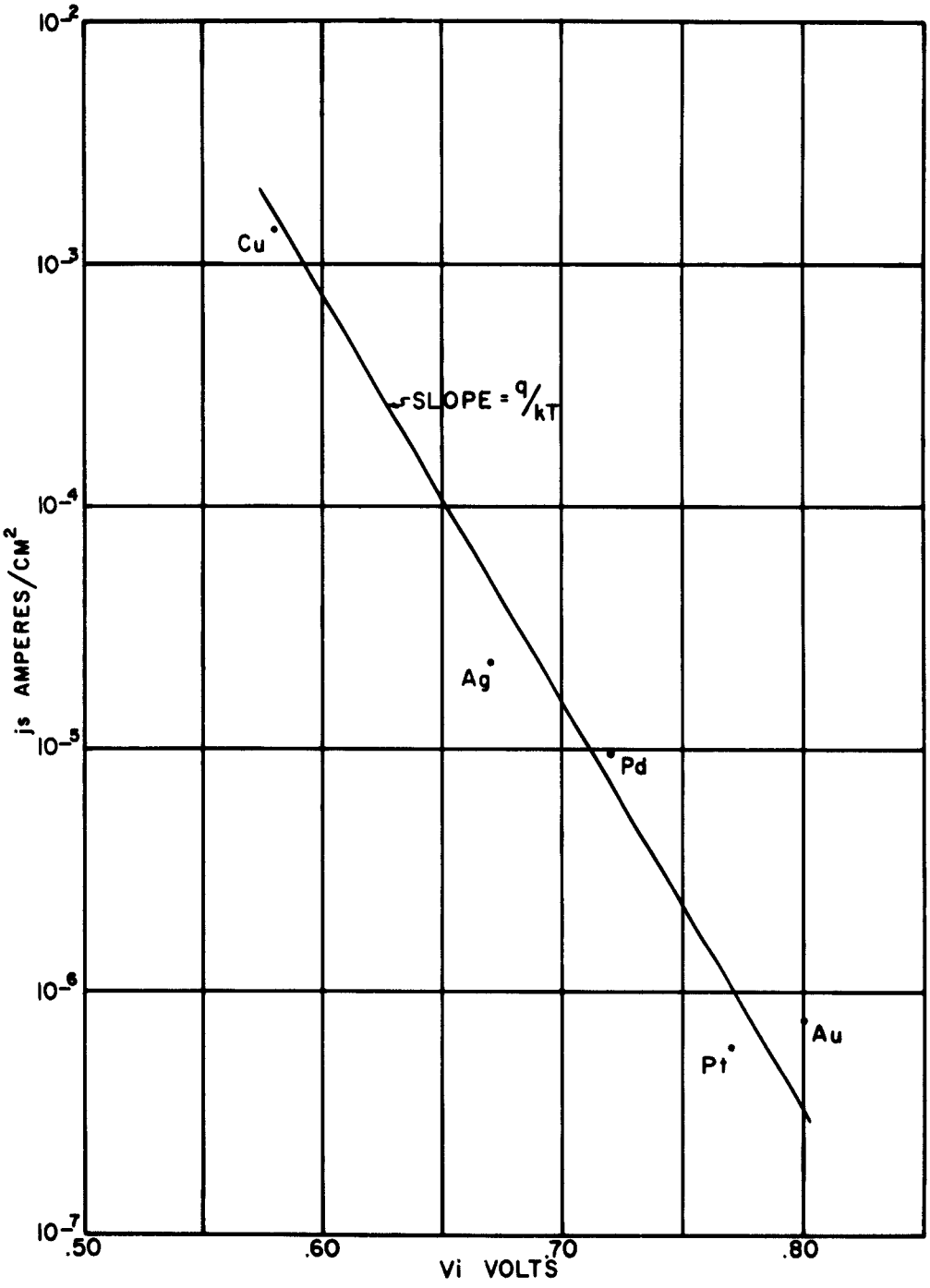
10^{-2}
10^{-3}
10^{-4}
10^{-5}
10^{-6}
10^{-7}
js AMPERES/CM^2
Cu
SLOPE = q/kT
Ag
Pd
Pt
Au
.50
.60
.70
.80
Vi VOLTS

Figure 19

TYPICAL TRIODE STRUCTURE

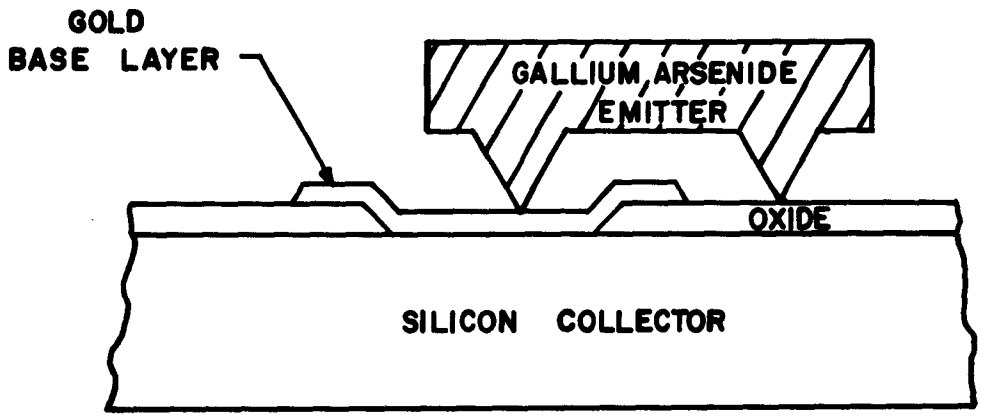

Figure 20

COLLECTOR CHARACTERISTICS OF Si-Au-Si TRIODE

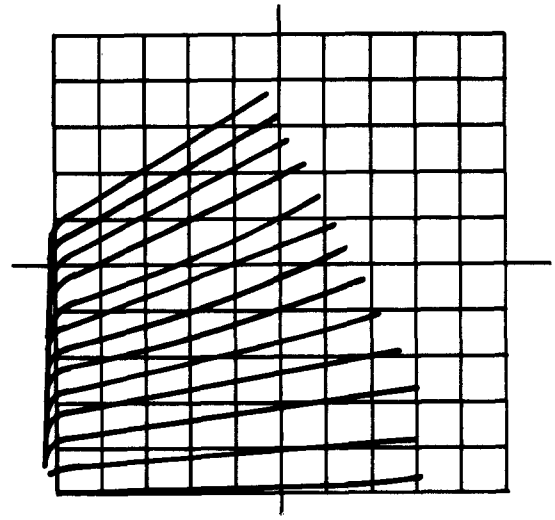

I_C
.01 ma/div

Vcb, 1V/DIV

BASE CURRENT .02 ma/STEP

Si-Au-Si TRIODE GROUNDED BASE

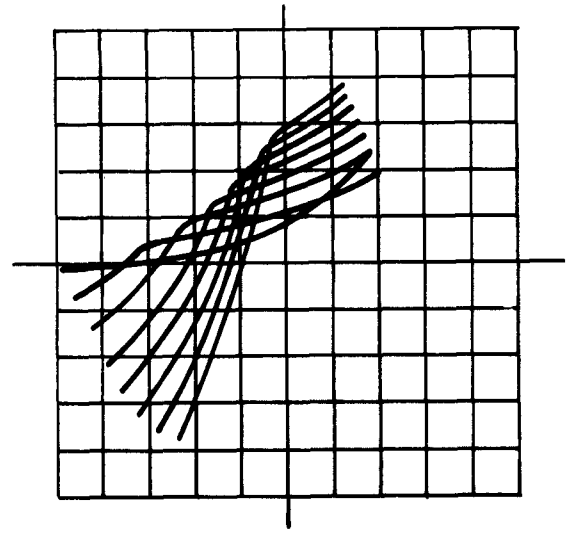

I_C
.02ma/div

Vce, 2V/DIV

BASE CURRENT .02 ma/STEP

Si-Au-Si TRIODE GROUNDED EMITTER

Figure 21

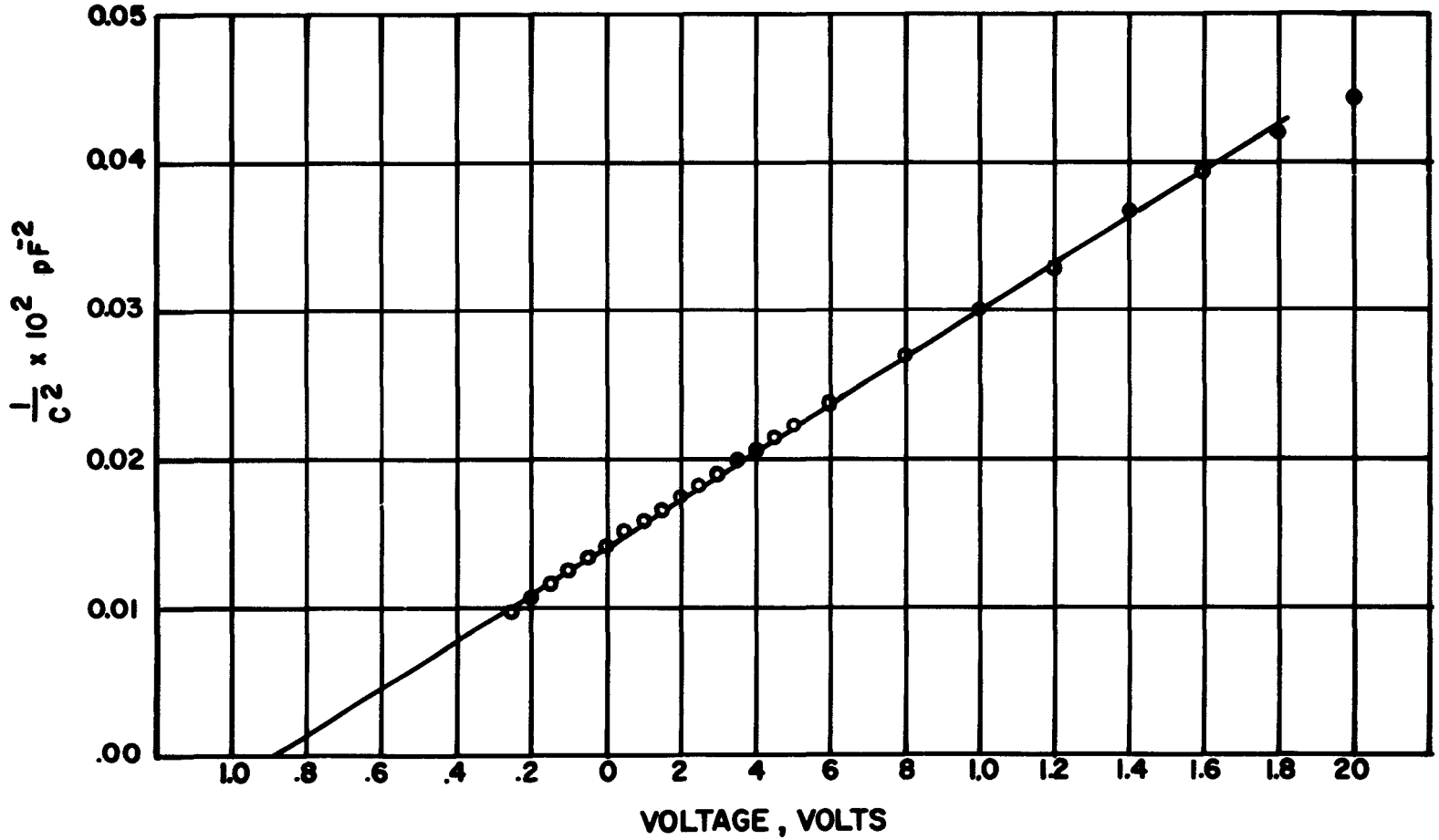
0.05
0.04
0.03
0.02
0.01
.00
$\frac{1}{C^2} \times 10^2$ pF^{-2}
1.0
.8
.6
.4
.2
0
2
4
6
8
1.0
1.2
1.4
1.6
1.8
20
VOLTAGE, VOLTS

Figure 22

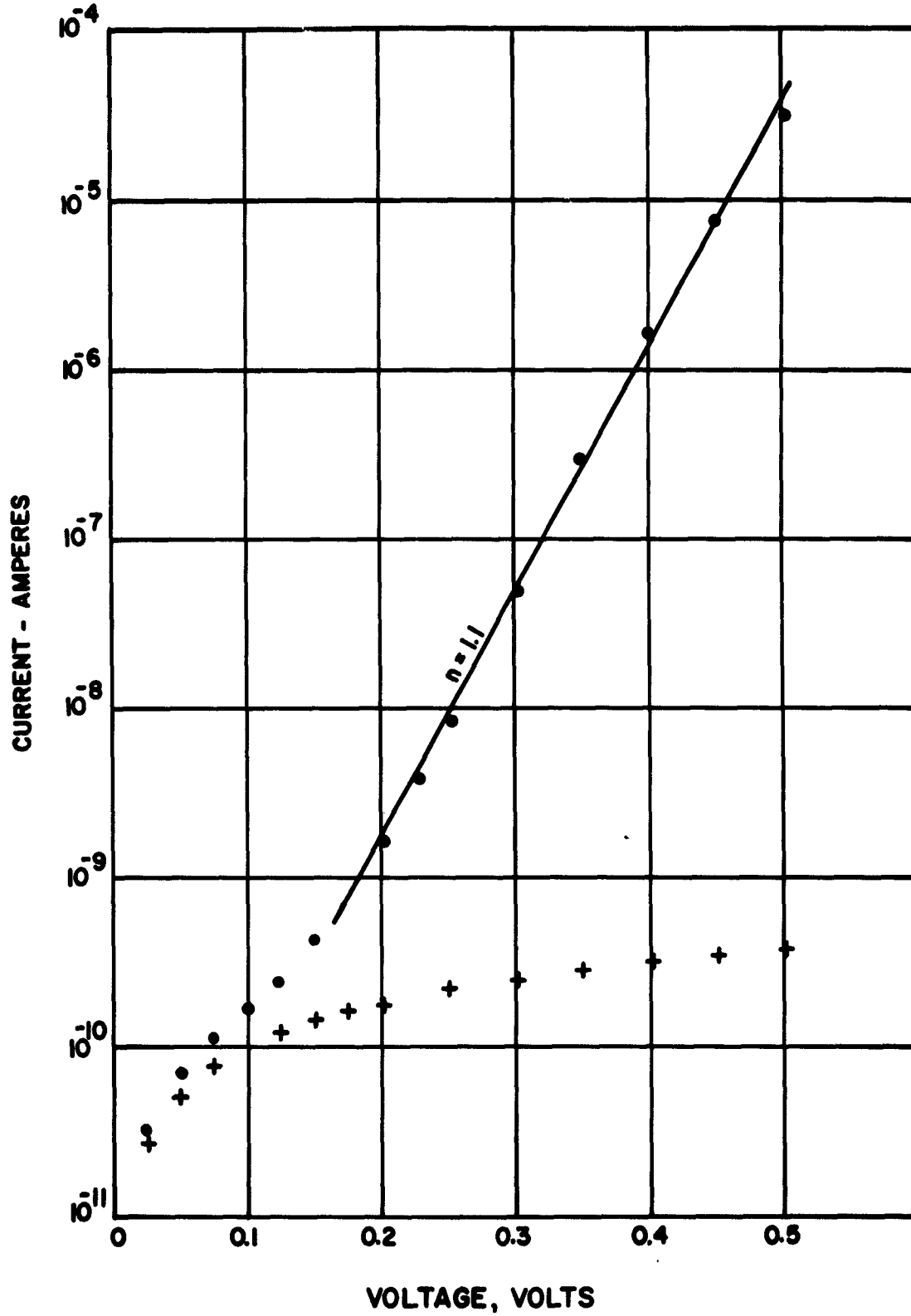
CURRENT - AMPERES
10⁻⁴
10⁻⁵
10⁻⁶
10⁻⁷
10⁻⁸
10⁻⁹
10⁻¹⁰
10⁻¹¹
n = 1.1
0
0.1
0.2
0.3
0.4
0.5
VOLTAGE, VOLTS

Figure 23

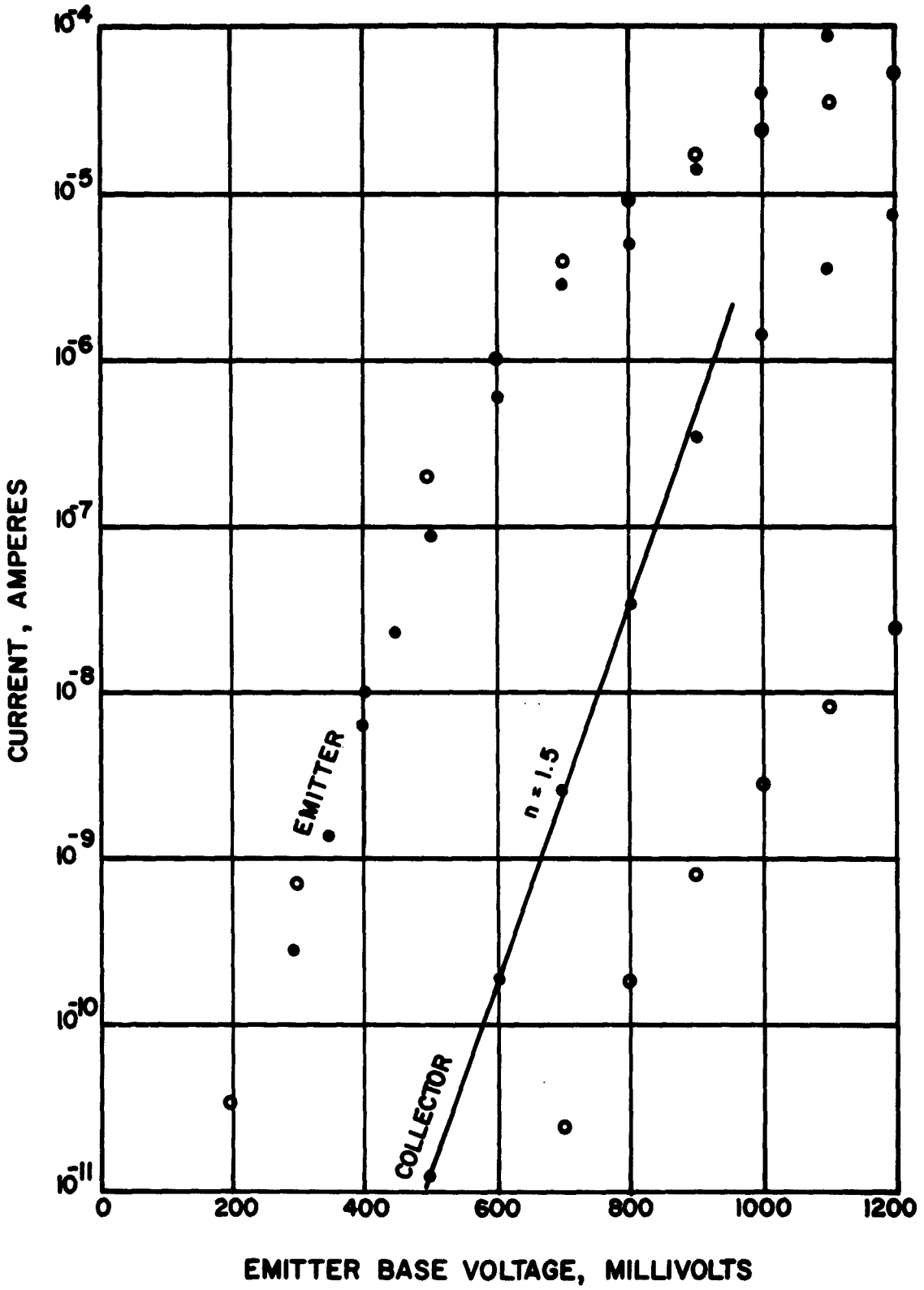
CURRENT, AMPERES
10^{-4}
10^{-5}
10^{-6}
10^{-7}
10^{-8}
10^{-9}
10^{-10}
10^{-11}
0
200
400
600
800
1000
1200
EMITTER BASE VOLTAGE, MILLIVOLTS
EMITTER
COLLECTOR
n = 1.5

Figure 24

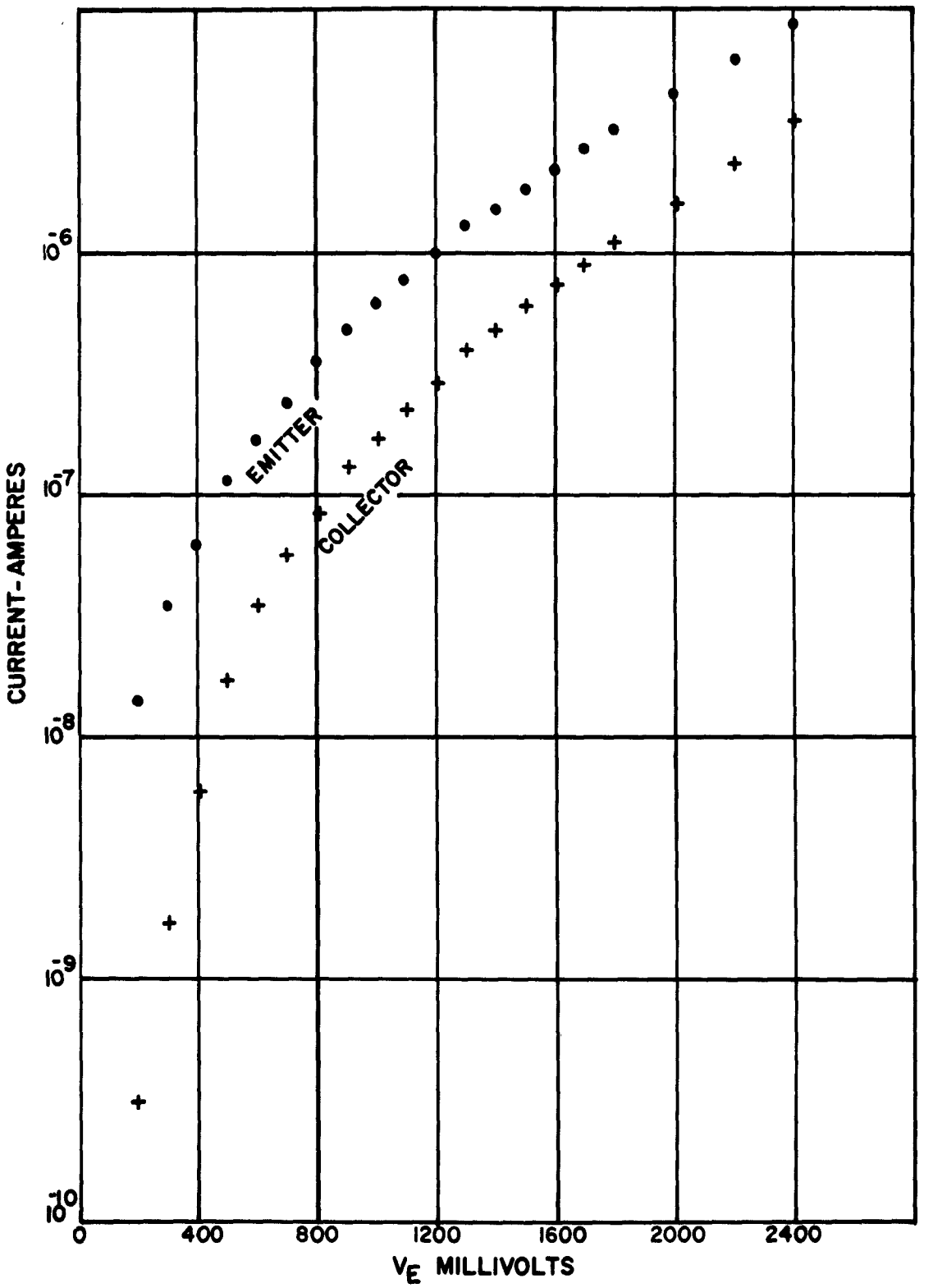
CURRENT-AMPERES
10^{-6}
10^{-7}
10^{-8}
10^{-9}
10^{-10}
EMITTER
COLLECTOR
0
400
800
1200
1600
2000
2400
V_E MILLIVOLTS

Figure 25

COLLECTOR CHARACTERISTICS OF GaAs-Au-Si TRIODE

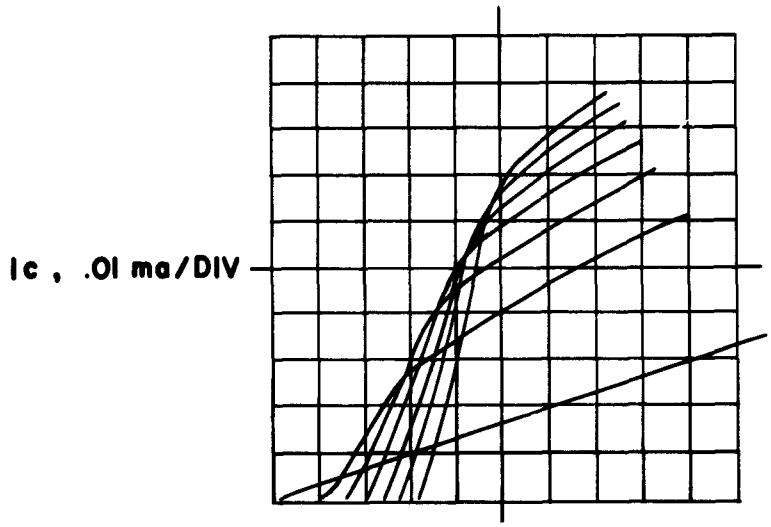

Figure 26

DISTRIBUTION

Code	Organization	No. of Copies
AF 5	AFMTC (AFMTC Tech. Library-MU-135) Patrick Air Force Florida	1
AF 18	AUL Maxwell Air Force Base Alabama	1
AF 32	OAR (PROS, Col. John R. Fowler) Tempo D 4th & Independence Avenue Washington 25, D. C.	1
AF 33	AFOSR, OAR (SRYP) Tempo D 4th & Independence Avenue Washington 25, D. C.	1
AF 43	ASD (ASAPRD - Dist) Wright-Patterson Air Force Base Ohio	1
AF 124	Rome Air Development Center (RAALD) Attn: Documents Library Griffiss Air Force Base New York	1
AF 139	Air Force Missile Development Center (MDGRT) Holloman Air Force Base New Mexico	1
AF 314	Headquarters OAR (RROSP, Maj. Richard W. Nelson) Washington 25, D. C.	1
Ar 5	Commanding General USASRDL Attn: Technical Documents Center SIGRA/SL-ADT Fort Monmouth, New Jersey	1
Ar 9	Department of the Army Office of the Chief Signal Officer ATTN: SIGRD-4a-2 Washington 25, D. C.	1

Code	Organization	No. of Copies
Ar 50	Commanding Officer Attn: ORDTL-012 Diamond Ordnance Fuze Laboratories Washington 25, D. C.	1
Ar 67	Redstone Scientific Information Center U.S. Army Missile Command Redstone Arsenal, Alabama	1
G 31	Office of Scientific Intelligence Central Intelligence Agency 2430 E Street, N. W. Washington 25, D. C.	1
G 2	ASTIA (TIPAA) Arlington Hall Station Arlington 12, Virginia	17
G 68	Scientific and Technical Information Facility Attn: NASA Representative (S-AK/DL) P. O. Box 5700 Bethesda, Maryland	1
G 109	Director Langley Research Center National Aeronautics and Space Admin. Langley Field, Virginia	1
N 9	Chief, Bureau of Naval Weapons Department of the Navy Washington 25, D. C. Attn: DLI-31	2
N 29	Director (Code 2027) U. S. Naval Research Laboratory Washington 25, D. C.	2
I 292	Director, USAF Project RAND The Rand Corporation 1700 Main Street Santa Monica, California THRU: Air Force Liaison Office	1
M 6	A. F. Cambridge Research Laboratories OAR (CRXRA - Stop 39) L. G. Hanscom Field Bedford, Massachusetts	20

Code	Organization	No. of Copies
AF 253	Technical Information Office European Office, Aerospace Research Shell Building, 47 Cantersteen Brussels, Belgium	1
Ar 107	U.S. Army Aviation Human Research Unit U. S. Continental Army Command P. O. Box 428 Fort Rucker, Alabama ATTN: Maj. Arne H. Eliasson	1
G 8	Library Boulder Laboratories National Bureau of Standards Boulder, Colorado	2
M 63	Institute of Aerospace Sciences, Inc. 2 East 64th Street New York 21, New York ATTN: Librarian	1
M 84	A.F. Cambridge Research Laboratories OAR (CRXR, J. R. Marple) L. G. Hanscom Field Bedford, Massachusetts	1
N 73	Office of Naval Research Branch Office, London Navy 100, Box 39 F.P.O., New York, New York	7
U 32	Massachusetts Institute of Technology Research Laboratory Building 26, Room 327 Cambridge 39, Massachusetts ATTN: John H. Hewitt	1
U 431	Alderman Library University of Virginia Charlottesville, Virginia	1
G 9	Defence Research Member Canadian Joint Staff 2450 Massachusetts Avenue, N. W. Washington 8, D. C.	1
AF 318	Aero Research Laboratory (OAR) AROL Lib. AFL 2292, Building 450 Wright-Patterson Air Force Base Ohio	1

Code	Organization	No. of Copies
AF 137	Aeronautical Systems Division (ASRNEM, Mr. Richard Alberts) Wright-Patterson Air Force Base Ohio	1
Ar 83	USASRDL Attn: SIGRA/SL-PD, H. Jacobs Fort Monmouth, New Jersey	1
G 70	Advisory Group on Electron Devices (AGED) Office of the Director of Defense Res. and Eng. 346 Broadway, 8th Floor New York 13, New York	4
I 43	Radio Corporation of America RCA Laboratories Princeton, New Jersey ATTN: Dr. P. K. Weimer	1
I 44	Bell Telephone Laboratories, Inc. Murray Hill New Jersey ATTN: Dr. J. Early	1
I 46	Corning Glass Works Corning New York ATTN: Thomas C. MacAvoy	1
I 154	General Electric Research Laboratories P. O. Box 1088, River Road Nishayuna, New York ATTN: Dr. R. N. Hall	1
I 233	Philco Scientific Laboratories Blue Bell Pennsylvania ATTN: Mr. James Spratt	1
I 820	Raytheon Company, Research Division Seyon Street Waltham, Massachusetts ATTN: Jerome M. Lavine	1
I 821	Xerox Corporation Research & Engineering Center 800 Phillips Road Webster, New York ATTN: Dr. F. A. Schwertz Director of Applied Research	1

Code	Organization	No. of Copies
I 979	Radio Corporation of America RCA Laboratories Princeton, New Jersey ATTN: Dr. William Webster	1
M 60	Electronic Systems Division (ESRDE, Maj. James Van Horn) L. G. Hanscom Field Bedford, Massachusetts	1
N 2	Chief, Bureau of Ships Departmen of the Navy Washington 25, D. C. ATTN: Mr. A. H. Young, Code 681A1A	1
U 20	Niels I. Meyer Physics Department Technical University Solvgate 83 Copenhagen, Denmark	1
	Headquarters A.F. Cambridge Research Laboratories (CRVSA, Dr. A. C. Yang) L. G. Hanscom Field Bedford, Massachusetts	9

Office of Aerospace Research, Air Force Cambridge Research Laboratories, Bedford, Mass.
Rpt. No. AFCRL-63-113, INVESTIGATION OF HOT ELECTRON EMITTER; Scientific Report No. 3, Feb. 63; 21p., illus.

Unclassified Report

The electrical properties of gold-silicon barriers have been studied experimentally in some detail. The reverse leakage current of these barriers is shown to be caused by lowering of the barrier due to the image force effect. The thermal activation energy of the saturation current was found to be 0.799 eV, identical to the height of the Au-Si barrier. The barrier height, saturation current density, and ideality of Pt, Pd, Ag, Ni and Cu barriers to Si are also presented. Two methods for fabricating hot electron triodes are described. Large area structures, made by pressing together a silicon-gold-silicon sandwich, do not exhibit triode characteristics and are limited by particulate matter and deviations from flatness. Triodes with point contact emitters of silicon and gallium arsenide have been fabricated and their current-voltage characteristics are presented. Current transfer ratios as high as 0.75 have been observed.

UNCLASSIFIED

1. Transistors
2. Diodes (Semiconductor)
3. Semiconductors
4. Photoelectric Effect

I. AFSC Project 4608, Task 460804
II. Contract AF19(628)-1637
III. -hp associates- Palo Alto, Calif.
IV. Atalla, M. M.
V. In ASTIA collection

UNCLASSIFIED

Office of Aerospace Research, Air Force Cambridge Research Laboratories, Bedford, Mass.
Rpt. No. AFCRL-63-113, INVESTIGATION OF HOT ELECTRON EMITTER; Scientific Report No. 3, Feb. 63; 21p., illus.

Unclassified Report

The electrical properties of gold-silicon barriers have been studied experimentally in some detail. The reverse leakage current of these barriers is shown to be caused by lowering of the barrier due to the image force effect. The thermal activation energy of the saturation current was found to be 0.799 eV, identical to the height of the Au-Si barrier. The barrier height, saturation current density, and ideality of Pt, Pd, Ag, Ni and Cu barriers to Si are also presented. Two methods for fabricating hot electron triodes are described. Large area structures, made by pressing together a silicon-gold-silicon sandwich, do not exhibit triode characteristics and are limited by particulate matter and deviations from flatness. Triodes with point contact emitters of silicon and gallium arsenide have been fabricated and their current-voltage characteristics are presented. Current transfer ratios as high as 0.75 have been observed.

UNCLASSIFIED

1. Transistors
2. Diodes (Semiconductor)
3. Semiconductors
4. Photoelectric Effect

I. AFSC Project 4608, Task 460804
II. Contract AF19(628)-1637
III. -hp associates- Palo Alto, Calif.
IV. Atalla, M. M.
V. In ASTIA collection

UNCLASSIFIED